Magnetic phase diagram of $\nu=2$ quantum Hall systems

Kanako Yoshizawa and Kazuo Takayanagi
Department of Physics, Sophia University, 7-1 Kioi-cho, Chiyoda-ku, Tokyo 102, Japan
(Received 1 December 2008; revised manuscript received 30 January 2009; published 24 March 2009)

We present the magnetic phase diagram of the $\nu=2$ quantum Hall system on the whole (r_s, E_Z) plane. We fix the phase boundaries of the paramagnetic and ferromagnetic states by looking for a softening of spin-density excitations in the time-dependent Hartree-Fock theory. A nontrivial phase is obtained in the self-consistent Hartree-Fock theory for $r_s \sim 2$ and $E_Z \lesssim 0.06\hbar\omega_c$, where both the paramagnetic and ferromagnetic states show spin instability. We show that the obtained phase is the spin-density wave (SDW) state, and explain the mechanism how the SDW stabilizes.

DOI: 10.1103/PhysRevB.79.125321 PACS number(s): 73.43.Nq, 73.43.Lp, 73.20.−r, 21.60.Jz

I. INTRODUCTION

The two-dimensional (2D) electron system in a strong magnetic field, the quantum Hall system, has been a major interest in condensed-matter physics because the large degeneracy of each Landau level is expected to exhibit new physics in the presence of the strong Coulomb repulsion. By tilting the magnetic field, we can lift the degeneracy of up- and down-spin electrons, and can explore the system from a wider point of view.[1] Experimental investigations of these systems have been providing new insight into the correlation in the quantum Hall systems.[2–5] At the same time, a lot of efforts have been made theoretically to examine the excited as well as the ground state of the system.[6–14] At present, however, we are still waiting for a clear understanding even of the ground state of the system.

The two-dimensional electron gas (2DEG) with a neutralizing background is described by a single (Wigner-Seitz) parameter r_s, which is related to the electron density n by $1/n=\pi(r_s a_0)^2$ with a_0 being the Bohr radius. In a perpendicular magnetic field B, the kinetic energy is quantized into discrete Landau levels with equal spacing $\hbar\omega_c$, where $\omega_c = eB/mc$ is the cyclotron frequency of electron. Each Landau level (with a fixed spin direction) can accommodate electrons maximally at the density $1/(2\pi l^2)$, where $l=\sqrt{\hbar c/eB}$ is the magnetic length. Then we define the filling factor $\nu = n/(2\pi l^2)$ for a system specified by the density n of electrons per unit area. By tilting the magnetic field, we can introduce another independent parameter E_Z, the Zeeman splitting energy, because E_Z is determined by the magnetic field B itself while ω_c is fixed by its normal component. Therefore, the quantum Hall system in a tilted magnetic field may be specified by three parameters: the Wigner-Seitz parameter r_s, the filling factor ν, and the Zeeman energy E_Z.

In this work, we concentrate on the integer quantum Hall system with $\nu=2$ on the (r_s, E_Z) plane. Figure 1 summarizes the current knowledge of the phase diagram. In the small r_s and small E_Z region, we expect that the paramagnetic phase $|\mathrm{P}\rangle$ $(\nu_\uparrow=\nu_\downarrow=1)$ would be the ground state. On the other hand, in the large r_s or large E_Z region, the system will be the ferromagnetic state $|\mathrm{F}\rangle$ $(\nu_\uparrow=2, \nu_\downarrow=0)$. Between these two limits has been the unknown area. At present, only two boundaries can be drawn in the phase diagram. One is the boundary of the first-order transition between $|\mathrm{P}\rangle$ and $|\mathrm{F}\rangle$ for $E_Z \sim \hbar\omega_c$ in the high-density $(r_s \ll 1)$ region.[6–8,10] This is understandable from Fig. 2 that depicts the situation with $r_s=0$; the system makes a transition from $|\mathrm{P}\rangle$ to $|\mathrm{F}\rangle$ as E_Z crosses $\hbar\omega_c$ from below. For a finite but small $r_s(\ll 1)$, the transition takes place at $E_Z < \hbar\omega_c$, which corresponds to the situation (b) in Fig. 2 due to the gain in the Coulomb exchange interaction in $|\mathrm{F}\rangle$. The other is the second-order boundary between $|\mathrm{P}\rangle$ and the spin-density wave (SDW) (Refs. 15 and 16) state at $r_s=2.01$ for $E_Z=0$,[14] which shall be explained later. Though other possibilities have been also suggested,[5,12,13,17–23] the phase diagram on the (r_s, E_Z) plane has not been known to date.

In this situation, we determine the phase diagram of the $\nu=2$ system on the whole (r_s, E_Z) plane in the framework of the self-consistent Hartree-Fock (HF) theory. To complete Fig. 1, we answer the following questions in this work. Where are the boundaries between $|\mathrm{P}\rangle$, $|\mathrm{F}\rangle$, and the SDW? Does $|\mathrm{F}\rangle$ show the spin instability as $|\mathrm{P}\rangle$ does? If so, what is the new phase implied by the instability? Our main findings and the answers to the above questions shall be summarized by the phase diagram in Fig. 27 that displays all possible phases and their boundaries on the (r_s, E_Z) plane. We shall see that the main features of the phase diagram are (i) a first-order boundary between $|\mathrm{P}\rangle$ and $|\mathrm{F}\rangle$ in the large E_Z region and (ii) a second-order boundary between $|\mathrm{P}\rangle$ and the SDW, and a first-order boundary between $|\mathrm{F}\rangle$ and the SDW, in the small E_Z region.

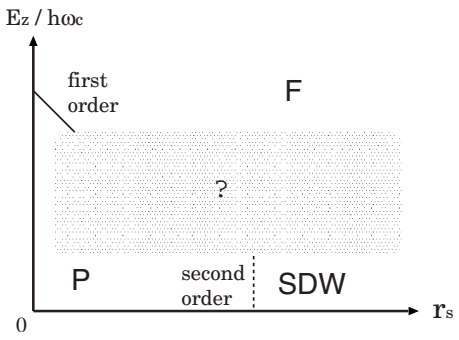

FIG. 1. Current knowledge of the phase diagram in the mean-field theory. Only two boundaries are known; one is the first-order boundary between $|\mathrm{P}\rangle$ and $|\mathrm{F}\rangle$ for $E_Z \sim \hbar\omega_c$ and $r_s \ll 1$. The other is the second-order boundary between $|\mathrm{P}\rangle$ and SDW at $r_s=2.01$ for $E_Z=0$. Unknown region is shown as a shaded area with a question mark.

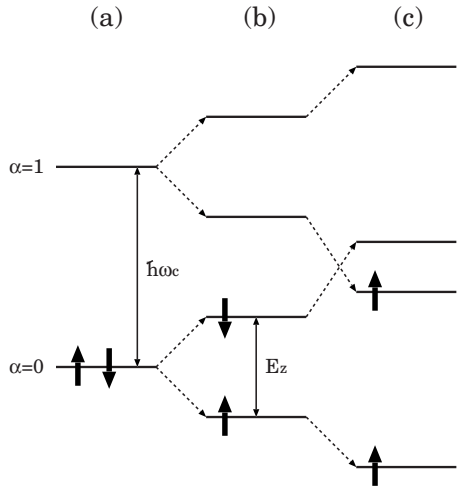

FIG. 2. Effect of Zeeman splitting E_Z on the $\nu=2$ system at $r_s=0$ (without Coulomb interaction between electrons). As E_Z increases, the system changes from (a) the paramagnetic state $|\mathrm{P}\rangle$ $(\nu_\uparrow=\nu_\downarrow=1)$ to (c) the ferromagnetic state $|\mathrm{F}\rangle$ $(\nu_\uparrow=2,\nu_\downarrow=0)$. (a): $|\mathrm{P}\rangle$ for $E_Z=0$. (b): $|\mathrm{P}\rangle$ for $E_Z\neq 0$. (c): $|\mathrm{F}\rangle$. Landau index is denoted as $\alpha=0,1$.

In principle, phase boundaries in the HF theory could be fixed by comparing energies of all possible HF solutions. Without any insight into the ground state, however, it is almost impossible to find HF solutions. We take, therefore, another way; we study dispersions of excited states on a HF solution to fix its boundary in the phase diagram. A vanishing excitation energy of a collective boson in the time-dependent Hartree-Fock (TDHF) theory means that the assumed ground state is no more the lowest energy Slater determinant. The most promising excitation mode is obviously the spin-density excitation (SDE).[6,12,14,19,20] In this case, the new ground state can be described as a condensate of the SDE boson with the vanishing excitation energy in a first approximation.[24] This is sufficient to perform the HF calculation to obtain the exact form of the new ground state, which shall be shown to be the SDW state.

We start with the two trivial HF solutions $|\mathrm{P}\rangle$ and $|\mathrm{F}\rangle$. Then we examine the SDE spectra on $|\mathrm{P}\rangle$ and $|\mathrm{F}\rangle$, and find the spin instability that signals a new HF ground state. As a result, we end up with four solutions to the HF equation: the paramagnetic state $|\mathrm{P}\rangle$, the SDW state $|\mathrm{SDW(P)}\rangle$ that originates from $|\mathrm{P}\rangle$, the ferromagnetic state $|\mathrm{F}\rangle$, and the SDW state $|\mathrm{SDW(F)}\rangle$ that derives from $|\mathrm{F}\rangle$. By comparing energies of these four solutions, we determine the ground state on the whole (r_s,E_Z) plane.

The plan of the paper is the following. In Sec. II, we briefly present general arguments on the HF and the TDHF theories to describe the ground and the excited states, respectively. In Sec. III, we discuss the spin instability of $|\mathrm{P}\rangle$ and $|\mathrm{F}\rangle$ for $E_Z=0$. Then we determine the ground state for $E_Z=0$ in Sec. IV. Here we show that the SDW is the ground state for $2.01<r_s<2.15$, and explain in detail how the SDW gains energy. We generalize the analysis in Secs. III and IV to $E_Z\neq 0$ systems in Secs. V and VI, respectively. In Sec. VII, we make discussions on the basis of our results. Here we show the main result of the present work, the phase diagram on the whole (r_s,E_Z) plane in Fig. 27. Then we compare our results with other theoretical approaches and experimental results. In Sec. VIII, we present conclusions.

II. FORMALISM

In this section, we explain the general formalism to describe the instability of $|\mathrm{P}\rangle$ and its resultant appearance of the SDW for $E_Z=0$. The theoretical framework is the HF theory[14,16,24] and the TDHF theory.[16,20,24] We shall see that the extension of the framework to the analysis of $|\mathrm{F}\rangle$ or $E_Z\neq 0$ cases is straightforward.

A. Landau level

We consider the integer quantum Hall system in the xy plane of size $L\times L$, which is described by the following Hamiltonian:

$$H=\sum_i \frac{1}{2m}\left(\boldsymbol{p}_i+\frac{e}{c}\boldsymbol{A}(\boldsymbol{r}_i)\right)^2+\frac{1}{2}\sum_{i\neq j}\frac{e^2}{|\boldsymbol{r}_i-\boldsymbol{r}_j|^2}. \tag{1}$$

We choose the Landau gauge, $\boldsymbol{A}=(0,Bx)$, to describe an electron of charge $-e$ in the xy plane with a magnetic field B in the z direction. Note that the ratio of the average electron-electron interaction, e^2/l, to the quanta of the kinetic energy, $\hbar\omega_c$, is given by

$$\frac{e^2/l}{\hbar\omega_c}=\frac{l}{a_0}=\sqrt{\frac{\nu}{2}}r_s. \tag{2}$$

For the $\nu=2$ system that we investigate in this work, the ratio is given just by r_s.

Now, we define the complete set of single-particle states by

$$\frac{1}{2m}\left(\boldsymbol{p}+\frac{e}{c}\boldsymbol{A}\right)^2\psi_{\alpha k}(\boldsymbol{r})=\varepsilon_\alpha^{(0)}\psi_{\alpha k}(\boldsymbol{r}), \tag{3}$$

where the Landau-level wave function is given by

$$\psi_{\alpha k}(\boldsymbol{r})=\frac{e^{iky}}{\sqrt{L}}\phi_\alpha(x+kl^2), \tag{4}$$

where $\alpha=0,1,\ldots$ is the Landau index. Here, ϕ_α is a one-dimensional harmonic-oscillator eigenstate with oscillator frequency ω_c, and $\varepsilon_\alpha^{(0)}=\hbar\omega_c(\alpha+\frac{1}{2})$. The single-particle basis, which is specified by the orbital and the spin part, is then given in the second quantized form as $\{a_{\alpha\sigma}^\dagger(k)|0\rangle\}$, where $\sigma=\uparrow,\downarrow$ stands for spin direction.

B. Excited state

Here we explain the description of excited states on $|\mathrm{P}\rangle$ in the TDHF framework. We are interested in excitations on $|\mathrm{P}\rangle$ that exhibit softening and therefore signal the instability of $|\mathrm{P}\rangle$. In this work, we examine the SDE, which are excited by $\sigma_\mp e^{i\boldsymbol{q}\cdot\boldsymbol{r}}$, because the charge-density excitation (CDE) excited by $e^{i\boldsymbol{q}\cdot\boldsymbol{r}}$ has much higher excitation energy than the SDE due to the direct repulsive particle-hole (ph) interaction.[5,12,13,19,20,22]

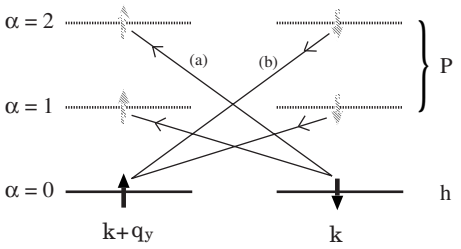

FIG. 3. Excitations induced by $\sigma_+(\boldsymbol{q})$ on $|\mathrm{P}\rangle$ with $\nu=2$. Landau indices are denoted by α. Solid and hatched arrows represent, respectively, occupied and unoccupied spin states in $|\mathrm{P}\rangle$. For the $\nu=2$ system, Landau indices h and p in the text are given by $h=0$ and $p=1,2,\ldots$, as indicated in the figure. Excitations by the first and the second terms in Eq. (6) correspond to the lines denoted by (a) and (b), respectively.

The external perturbation in the SDE channel, $\sigma_+(\boldsymbol{q})=\sigma_+e^{i\boldsymbol{q}\cdot\boldsymbol{r}}$ with wave number $\boldsymbol{q}=(q_x,q_y)$, is given in the second-quantized form as

$$\sigma_+(\boldsymbol{q})=\sum_{\alpha\beta}\sum_k a^\dagger_{\alpha\uparrow}(k+q_y)a_{\beta\downarrow}(k)e^{-i\phi(k)}F_{\alpha\beta}(\boldsymbol{q})$$

$$=\sum_{\alpha\beta}C_{\alpha\beta}(\boldsymbol{q})F_{\alpha\beta}(\boldsymbol{q}), \tag{5}$$

where $\phi(k)=(k+q_y/2)q_xl^2$, and $F_{\alpha\beta}(\boldsymbol{q})$ is defined in the Appendix. We have also defined $C_{\alpha\beta}(\boldsymbol{q})$ in the second line. Now we adopt the convention to use h and p, respectively, for the Landau indices of occupied and unoccupied states. For the paramagnetic state $|\mathrm{P}\rangle$ $(\nu_\uparrow=\nu_\downarrow=1)$, these Landau indices, h and p, take on $h=0$ and $p=1,2,\ldots$.

In the standard TDHF theory, we describe the creation operator of the nth excited state in the σ_+ SDE channel as

$$\mathcal{O}^{(n)}(\boldsymbol{q})=\sum_{ph}\{x^{(n)}_{ph}C_{ph}(\boldsymbol{q})-y^{(n)}_{ph}C_{hp}(\boldsymbol{q})\}, \tag{6}$$

where the first term describes ph excitations along the line (a) in Fig. 3, and the second term corresponds to the ph de-excitations along the line (b). Here the amplitudes $x^{(n)}_{ph}$ and $y^{(n)}_{ph}$ are determined by the TDHF equation in the following matrix form:

$$\begin{pmatrix} A(\boldsymbol{q}) & B(\boldsymbol{q}) \\ B^*(-\boldsymbol{q}) & A^*(-\boldsymbol{q}) \end{pmatrix}\begin{pmatrix} \mathcal{X}^{(n)} \\ \mathcal{Y}^{(n)} \end{pmatrix}=E^{(n)}\begin{pmatrix} \mathcal{X}^{(n)} \\ -\mathcal{Y}^{(n)} \end{pmatrix}, \tag{7}$$

where $E^{(n)}$ is the excitation energy of the nth excited state and the column vectors $\mathcal{X}^{(n)}$ and $\mathcal{Y}^{(n)}$ are specified by $\{\mathcal{X}^{(n)}\}_{ph}=x^{(n)}_{ph}$ and $\{\mathcal{Y}^{(n)}\}_{ph}=y^{(n)}_{ph}$, respectively. The matrices A and B are defined as

$$\{A(\boldsymbol{q})\}_{ph,p'h'}=(\varepsilon_p-\varepsilon_h)\delta_{p,p'}\delta_{h,h'}-X_{ph'p'h}(\boldsymbol{q}),$$

$$\{B(\boldsymbol{q})\}_{ph,p'h'}=-X_{pp'h'h}(\boldsymbol{q}), \tag{8}$$

where diagrammatic expressions for $X_{ph'p'h}(\boldsymbol{q})$ and $X_{pp'h'h}(\boldsymbol{q})$ are given in Fig. 4. Here, $X_{\alpha\alpha'\beta\beta'}(\boldsymbol{q})$ represents a special combination of the matrix elements of Coulomb interaction in the ph channel, and is defined in the Appendix. The HF single-particle energy is denoted by

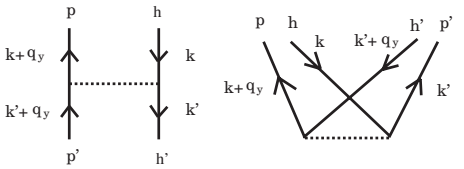

FIG. 4. Diagrammatic expression for the ph interaction in the $(ph,p'h')$ component of Eq. (8). Left: $X_{ph'p'h}(\boldsymbol{q})$ in matrix $A(\boldsymbol{q})$. Right: $X_{pp'h'h}(\boldsymbol{q})$ in matrix $B(\boldsymbol{q})$. See the Appendix for detail.

$$\varepsilon_\alpha=\varepsilon^{(0)}_\alpha+\Sigma^{\mathrm{HF}}_\alpha, \tag{9}$$

where $\Sigma^{\mathrm{HF}}_\alpha$ is the Fock exchange self-energy of level α shown in Fig. 5, and is given by

$$\Sigma^{\mathrm{HF}}_\alpha=-\sum_h X_{\alpha hh\alpha}(0). \tag{10}$$

We present several examples of $X_{\alpha\alpha'\beta\beta'}(0)$ explicitly in the Appendix.

To summarize, the lowest energy solution of Eq. (7) as a function of $q=|\boldsymbol{q}|$ for a fixed value of r_s determines the dispersion of the SDE.

C. Ground state

The paramagnetic state $|\mathrm{P}\rangle$ $(\nu_\uparrow=\nu_\downarrow=1)$ constitutes a solution to the HF equation for any value of r_s, and the same is true for the ferromagnetic state $|\mathrm{F}\rangle$ $(\nu_\uparrow=2,\nu_\downarrow=0)$. Suppose we solve Eq. (7) to obtain the excitation energy $E^{(n)}$ as a function of $q=|\boldsymbol{q}|$ for a fixed value of r_s. If $|\mathrm{P}\rangle$ is a stable Slater determinant for the fixed r_s, all the excitations would appear with real positive energies. Once we observe a vanishing excitation energy $(E^{(n)}\to 0)$, however, we need to search for a new ground state. Here the correspondence is exact; the vanishing excitation energy in the TDHF theory means that the assumed HF state is no more the local minimum on the energy surface spanned by Slater determinants, signaling a second-order transition to a new HF ground state.[16,24]

Now we are to search for the new HF ground state for each value of r_s, for which the SDE dispersion exhibits instability of $|\mathrm{P}\rangle$. This can be achieved using the density matrix in the following manner.[14]

Let us first denote the density matrix of an arbitrary Slater determinant $|\Psi\rangle$ as

$$\rho_{\alpha\sigma,\beta\tau}(k,k')=\langle\Psi|a^\dagger_{\beta\tau}(k')a_{\alpha\sigma}(k)|\Psi\rangle, \tag{11}$$

where $\rho^2=\rho$ is required for $|\Psi\rangle$ being a Slater determinant.[16,24] As an example, for the paramagnetic state

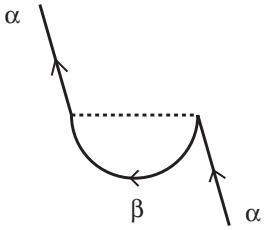

FIG. 5. Hartree-Fock exchange self-energy $\Sigma^{\mathrm{HF}}_\alpha$ of Eq. (10).

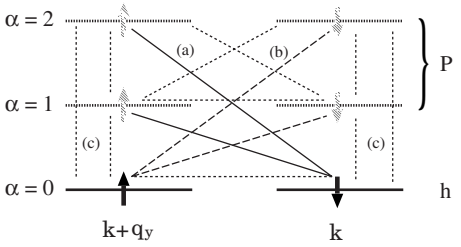

FIG. 6. Effects of spin fluctuations on the paramagnetic state $|\mathrm{P}\rangle$ with $\nu=2$. Lines denoted by (a), (b), and (c) indicate mixing of single-particle states induced by the self-consistent HF calculation. (a): mixing in the zeroth order in the Coulomb interaction. (b): mixing in the first order. (c): mixing in the second order. Notation is the same as for Fig. 3.

$|\Psi\rangle=|\mathrm{P}\rangle$ with $\nu=2$, where single-particle states created by $a_{0\uparrow}^{\dagger}(k)$ and $a_{0\downarrow}^{\dagger}(k)$ with all possible k values are occupied, the only nonzero element of the density matrix is given by $\rho_{0\sigma,0\sigma}(k,k)=1$ for $\sigma=\uparrow,\downarrow$.

Let $|\Psi\rangle$ be the new HF ground state which replaces $|\mathrm{P}\rangle$. Then the general form of the density matrix of $|\Psi\rangle$ can be deduced by examining the effect of $\sigma_{+}(\boldsymbol{q})$ on $|\mathrm{P}\rangle$. It is easily seen that $\sigma_{+}(\boldsymbol{q})$ first mixes single-particle states along the line (a) in Fig. 6 to induce a component $a_{p\uparrow}^{\dagger}(k+q_y)a_{h\downarrow}(k)|\mathrm{P}\rangle$ in $|\Psi\rangle$. This in turn gives a nonzero value to the matrix element

$$\rho_{p\uparrow,h\downarrow}(k+q_y,k)=\langle\Psi|a_{h\downarrow}^{\dagger}(k)a_{p\uparrow}(k+q_y)|\Psi\rangle, \tag{12}$$

and its Hermitian conjugate in the first order of the external perturbation. This is not, however, the whole story. The above element of ρ immediately gives a mean field that mixes single-particle states along the line (b), and then (c) in Fig. 6. Note that the condensate of the SDE boson in the σ_{+} channel necessarily makes a mean field that produces a mixture of states along the line (b) and therefore the condensate of σ_{-} SDE boson. A little consideration along the above line shows that the density matrix should have the following structure for each combination of Landau indices $\alpha\beta$ and wave number k:

$$\rho=\begin{pmatrix}\rho_{\alpha\uparrow,\beta\uparrow}(k+q_y,k+q_y) & \rho_{\alpha\uparrow,\beta\downarrow}(k+q_y,k)\\ \rho_{\alpha\downarrow,\beta\uparrow}(k,k+q_y) & \rho_{\alpha\downarrow,\beta\downarrow}(k,k)\end{pmatrix}. \tag{13}$$

Then, a straightforward calculation in the standard HF framework shows that the single-particle HF Hamiltonian has exactly the same structure as that of ρ of Eq. (13) to give

$$h=\begin{pmatrix}h_{\alpha\uparrow,\beta\uparrow}(k+q_y,k+q_y) & h_{\alpha\uparrow,\beta\downarrow}(k+q_y,k)\\ h_{\alpha\downarrow,\beta\uparrow}(k,k+q_y) & h_{\alpha\downarrow,\beta\downarrow}(k,k)\end{pmatrix}, \tag{14}$$

where each component is given by

$$h_{\alpha\uparrow,\beta\uparrow}=\varepsilon_{\alpha}\delta_{\alpha\beta}-X_{\alpha\alpha'\beta'\beta}(0)\rho_{\beta'\uparrow,\alpha'\uparrow}, \tag{15}$$

$$h_{\alpha\uparrow,\beta\downarrow}=-X_{\alpha\alpha'\beta'\beta}(\boldsymbol{q})\rho_{\beta'\uparrow,\alpha'\downarrow}, \tag{16}$$

$$h_{\alpha\downarrow,\beta\uparrow}=-X_{\alpha'\alpha\beta\beta'}(\boldsymbol{q})\rho_{\beta'\downarrow,\alpha'\uparrow}, \tag{17}$$

$$h_{\alpha\downarrow,\beta\downarrow}=\varepsilon_{\alpha}\delta_{\alpha\beta}-X_{\alpha\alpha'\beta'\beta}(0)\rho_{\beta'\downarrow,\alpha'\downarrow}. \tag{18}$$

Here repeated Landau indices are assumed to be summed over the whole model space, and the arguments of ρ and h are specified by Eqs. (13) and (14), respectively. Now we can write the HF eigenvalue equation in this system as

$$\sum_{\beta\tau}h_{\alpha\sigma,\beta\tau}D_{\beta\tau,j}=\epsilon_j D_{\alpha\sigma,j},\quad j=1,2,\ldots, \tag{19}$$

which gives jth eigenenergy ϵ_j and the corresponding eigenvector $D_{\alpha\sigma,j}$. The HF ground state $|\Psi\rangle$ can be obtained by filling the lowest ν eigenstates $(j=1,\ldots,\nu)$ of Eq. (19). These new single-particle states are created by the following operators specified by $D_{\alpha\sigma,j}$:

$$c_j^{\dagger}(k)=\sum_{\alpha}\{a_{\alpha\uparrow}^{\dagger}(k+q_y)D_{\alpha\uparrow,j}+a_{\alpha\downarrow}^{\dagger}(k)D_{\alpha\downarrow,j}\}. \tag{20}$$

Then the density matrix of Eq. (13) can be given as

$$\rho_{\alpha\sigma,\beta\tau}=\sum_{j}D_{\alpha\sigma,j}D_{\beta\tau,j}^{*}. \tag{21}$$

Note that the new basis $\{c_j^{\dagger}(k)|0\rangle\}$ is defined as a mixture of up- and down-spin states as is clear from Eq. (20), it implies that the new HF state obtained here is featured by the spin densities

$$\langle\psi_{\uparrow}^{\dagger}(\boldsymbol{r})\psi_{\uparrow}(\boldsymbol{r})\rangle=\frac{1}{2\pi l^2}\sum_{\alpha}\rho_{\alpha\uparrow,\alpha\uparrow},$$

$$\langle\psi_{\uparrow}^{\dagger}(\boldsymbol{r})\psi_{\downarrow}(\boldsymbol{r})\rangle=\sum_{\alpha,\beta}\rho_{\beta\downarrow\alpha\uparrow}\frac{1}{2\pi l^2}F_{\alpha\beta}(\boldsymbol{q})e^{-i\boldsymbol{q}\cdot\boldsymbol{r}}. \tag{22}$$

These expressions show that $\langle\sigma_z\rangle$ is a constant in space, and $\langle\sigma_x\rangle$ and $\langle\sigma_y\rangle$ show a spiral structure with the wave number $\boldsymbol{q}$, indicating that the new HF state is a spiral SDW state.[16]

The expectation value of the Hamiltonian, $\langle\Psi|H|\Psi\rangle$, of a Slater determinant $|\Psi\rangle$ is a function of the density matrix ρ.[16,24] Then the total energy per particle, $E[\rho]$, reads

$$\begin{aligned}E[\rho]&=\frac{1}{N}\langle\Psi|H|\Psi\rangle=\frac{1}{\nu}\sum_{\alpha}\sum_{\sigma}\varepsilon_{\alpha}^{(0)}\rho_{\alpha\sigma,\alpha\sigma}\\&-\frac{1}{2\nu}\sum_{\substack{\alpha,\alpha'\\ \beta,\beta'}}\sum_{\sigma}\rho_{\beta'\sigma,\alpha\sigma}\rho_{\beta\sigma,\alpha'\sigma}X_{\alpha\alpha'\beta\beta'}(0)\\&-\frac{1}{\nu}\sum_{\substack{\alpha,\alpha'\\ \beta,\beta'}}\rho_{\beta'\downarrow,\alpha\uparrow}\rho_{\beta\uparrow,\alpha'\downarrow}X_{\alpha\alpha'\beta\beta'}(\boldsymbol{q})=E_1+E_2+E_3,\end{aligned} \tag{23}$$

which stands for the total energy per electron [$N=\nu L^2/(2\pi l^2)$ being the total number of electrons]. In the last line, we have defined E_1, E_2, and E_3 for later use. Here E_1 is the kinetic energy and E_2+E_3 is the exchange energy in terms of the new basis states of Eq. (20). Note that E_3 derives from the mixture of single-particle states with momentum $k+q_y$ and k in Eq. (20), and is absent for $|\mathrm{P}\rangle$.

To summarize, we have presented the HF theory to describe the SDW ground state in terms of the density matrix. The minimum of $E[\rho]$ of Eq. (23) subject to $\rho^2=\rho$ can now be obtained by the self-consistent solution of Eqs. (15)–(19) and (21). The solution should be the SDW state where $|\mathrm{P}\rangle$ exhibits spin instabilities.

At the end, we emphasize that $X_{\alpha\alpha'\beta\beta'}(\boldsymbol{q})$ of Eqs. (A7) and (A8), which is a special combination of the matrix elements of Coulomb interaction, appears in Eq. (7) in the study of the excited states, and in Eqs. (14) and (23) in the study of the SDW ground state. This fact clearly indicates that the softening of the SDE and the stabilization of the SDW phase can be investigated in a unified way in terms of $X_{\alpha\alpha'\beta\beta'}(\boldsymbol{q})$, the exchange interaction defined in the *ph* channel.

D. Numerical recipes

Here we make several points on numerical calculations for the $\nu=2$ system. In the TDHF calculation, the model space to give convergent results depends on r_s and q. For $r_s\sim 1$, where the correlation is weak, the model space with the lowest three or four Landau levels is sufficient up to $q\sim 4l^{-1}$. On the other hand, for $r_s\sim 5$, we need the lowest seven or eight Landau levels to achieve convergence in the same region of q.

Another point is on the phase. There are several phase factors in the formulas we have presented. In Eq. (5), for example, we have the k-dependent phase factor $\phi(k)=(k+q_y/2)q_x l^2$. In the definition of $F_{\alpha\beta}(\boldsymbol{q})$ and $X_{\alpha\alpha'\beta\beta'}(\boldsymbol{q})$ given in the Appendix, we have products of phase factors of the form $\mathcal{N}_\alpha=i^\alpha e^{-i\alpha\theta}$, where θ is defined as $\boldsymbol{q}=(q_x,q_y)=(q\cos\theta, q\sin\theta)$. Though physical quantities such as excitation spectra or the ground-state energy do not depend on θ,[13,14] these phase factors enter the density matrix ρ of Eq. (13) and therefore the HF Hamiltonian h of Eq. (14). In order to get rid of these phase factors in what follows, we fix the external momentum $\boldsymbol{q}$ in the y direction, $\boldsymbol{q}=(0,q)$, i.e., $\theta=\pi/2$, so that we have $\phi(k)=0$ and $\mathcal{N}_\alpha=1$. Then we can show easily that ρ of Eq. (13) is independent of k, and the same is true for h of Eq. (14). Another merit of this convention ($\theta=\pi/2$) is that $X_{\alpha\alpha'\beta\beta'}(\boldsymbol{q})=X_{\alpha\alpha'\beta\beta'}(q)$ becomes a real quantity, as can be seen from Eq. (A10), which allows us to use real quantities only.

III. INSTABILITY FOR $E_Z=0$

In this section, we examine possible softening of the SDE on $|\mathrm{P}\rangle$ and $|\mathrm{F}\rangle$ in the TDHF framework for $E_Z=0$.

A. Instability of $|\mathrm{P}\rangle$

Let us first note that the total energy per particle, E_P, of $|\mathrm{P}\rangle$, which is characterized by the nonzero element $\rho_{0\sigma,0\sigma}(k,k)=1$ for $\sigma=\uparrow,\downarrow$, is given by Eq. (23) as

$$E_\mathrm{P}=\frac{1}{2}\hbar\omega_c-\frac{1}{2}X_{0000}(0)=\frac{1}{2}\hbar\omega_c\left(1-\sqrt{\frac{\pi}{2}}r_s\right), \quad (24)$$

where we have used Eqs. (2) and (A13). We also notice that the HF single-particle energy of Eq. (9) reads

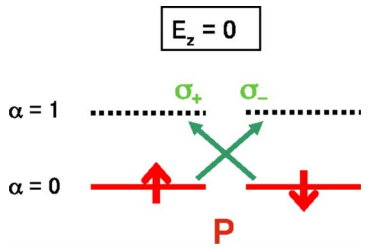

FIG. 7. (Color online) Schematical expression for the SDE in the σ_+ and σ_- channels. These two channels are degenerate for $E_Z=0$.

$$\varepsilon_{0\uparrow}=\varepsilon_{0\downarrow}=\hbar\omega_c\left(\frac{1}{2}-\sqrt{\frac{\pi}{2}}r_s\right),$$

$$\varepsilon_{1\uparrow}=\varepsilon_{1\downarrow}=\hbar\omega_c\left(\frac{3}{2}-\frac{1}{2}\sqrt{\frac{\pi}{2}}r_s\right). \quad (25)$$

Now we examine the SDE. In Fig. 7, we show a schematical expression for the SDE in the σ_+ and σ_- channels, which obviously give the same excitation spectra for $E_Z=0$. In the following we consider the SDE on $|\mathrm{P}\rangle$ in the σ_+ channel in the TDHF framework of Sec. II B.

Let us concentrate on the lowest energy SDE solution of Eq. (7), and denote its energy as $E^{(\mathrm{SDE})}$. In Fig. 8, we plot $E^{(\mathrm{SDE})}$ in units of $\hbar\omega_c$ for $r_s=1$ and 2. A particularly interesting feature of the SDE dispersion is the magnetoroton minimum that appears at a finite wave vector $q\sim 1.8l^{-1}$.[12,20] Figure 8 shows that the magnetoroton energy falls with decreasing density, ultimately to vanish at $r_s=2.01$, indicating instability of $|\mathrm{P}\rangle$ with respect to spin fluctuations induced by $\sigma_+ e^{i\boldsymbol{q}\cdot\boldsymbol{r}}$. This means that $|\mathrm{P}\rangle$ is a local minimum of $E[\rho]$ of Eq. (23) for $r_s<2.01$ only. For $r_s>2.01$, we shall find the SDW as the HF ground state in Sec. IV.

We can understand the above instability on the basis of the relevant *ph* interaction $-X_{\alpha\alpha'\beta\beta'}(\boldsymbol{q})$ which is shown in Fig. 9. The SDE in the first-order perturbation theory, as illustrated by the σ_+ line in Fig. 7, is featured by the following dispersion:[19]

$$E^{(\mathrm{SDE})}(1\mathrm{st\ \ order})=\hbar\omega_c-X_{1010}(\boldsymbol{q}).$$

We see that the dispersion for $r_s=1$ in Fig. 8 behaves in the same way as $-X_{1010}(\boldsymbol{q})$ in Fig. 9, showing that the above

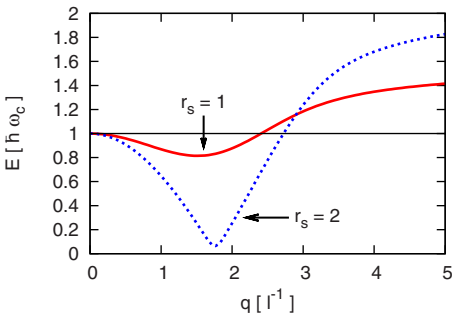

FIG. 8. (Color online) TDHF dispersion $E^{(\mathrm{SDE})}$ of the lowest SDE on $|\mathrm{P}\rangle$ in units of $\hbar\omega_c$ for $r_s=1$ and 2.

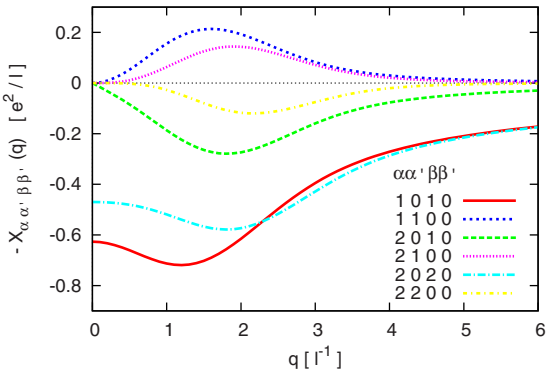

FIG. 9. (Color online) q dependence of the ph exchange interaction $-X_{\alpha\alpha'\beta\beta'}(\boldsymbol{q})$ in units of e^2/l for typical index sets $(\alpha\alpha'\beta\beta')$. Multiplying the displayed quantities by the ratio of Eq. (2), we can change the unit from e^2/l to $\hbar\omega_c$ for a system with any r_s. Note that the symmetry property of Eq. (A9) gives, e.g., $X_{1010}(\boldsymbol{q})=X_{0101}(\boldsymbol{q})$.

first-order perturbation theory works well for $r_s=1$.

As r_s increases, higher-order effects come into play. It is visible in Fig. 8 that the TDHF equation for $r_s=2$ enhances the effect of the attraction of $-X_{1010}(\boldsymbol{q})$ (see the left process in Fig. 4) in a nonlinear fashion around $q\sim 1.8l^{-1}$ to make the system unstable. The main driving force for this nonlinear effect comes from the ph interaction $-X_{1100}(\boldsymbol{q})$ in the matrix $B(\boldsymbol{q})$ in Eq. (7) (see the right process in Fig. 4), which has a maximum around $q\sim 1.7l^{-1}$ as shown in Fig. 9.

The above observation clearly explains (i) that the magnetoroton minimum in the small $r_s(\lesssim 1)$ region derives mainly from the strong attraction around $q\sim 1.3l^{-1}$ in the ph interaction $-X_{1010}(\boldsymbol{q})$ and (ii) that the spin instability at $r_s\sim 2$, which is a nonlinear phenomenon, originates from a cooperative effect of $-X_{1010}(\boldsymbol{q})$ and $-X_{1100}(\boldsymbol{q})$.

B. Instability of $|\mathrm{F}\rangle$

Here we investigate possible instabilities of the ferromagnetic state $|\mathrm{F}\rangle$ for $E_Z=0$. Let us first note that the energy E_F of $|\mathrm{F}\rangle$, which is characterized by the nonzero element $\rho_{\alpha\downarrow,\alpha\downarrow}(k,k)=1$ for $\alpha=0,1$, is given by Eq. (23) as

$$E_\mathrm{F}=\hbar\omega_c-\frac{1}{4}X_{0000}(0)-\frac{1}{2}X_{1001}(0)-\frac{1}{4}X_{1111}(0)$$
$$=\hbar\omega_c\left(1-\frac{11}{16}\sqrt{\frac{\pi}{2}}r_s\right), \tag{26}$$

where we have used Eq. (A13) in the Appendix.

Equations (24) and (26) give

$$E_\mathrm{F}-E_\mathrm{P}=\frac{1}{2}\hbar\omega_c\left(1-\frac{3}{8}\sqrt{\frac{\pi}{2}}r_s\right), \tag{27}$$

which implies that $E_\mathrm{P}\gtrless E_\mathrm{F}$ for $r_s\gtrless 2.13$. This shows explicitly that the increase $\hbar\omega_c/2$ in the kinetic energy in $E_\mathrm{F}-E_\mathrm{P}$ is compensated by the increase in the exchange interaction for $r_s>2.13$ to make $E_\mathrm{P}>E_\mathrm{F}$. Note that the stability of $|\mathrm{F}\rangle$ in the large r_s regime originates from the exchange interaction that operates between the same spin states only, but not from the Zeeman energy.

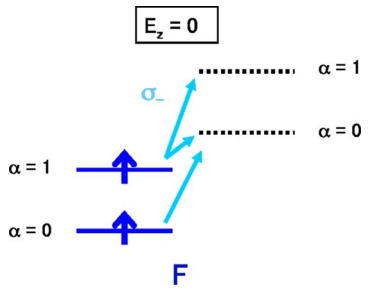

FIG. 10. (Color online) Schematical expression for the SDE on $|\mathrm{F}\rangle$ for $E_Z=0$.

Let us turn to the SDE on $|\mathrm{F}\rangle$. As shown schematically in Fig. 10, the relevant SDE is induced by $\sigma_- e^{i\boldsymbol{q}\cdot\boldsymbol{r}}$. Now we start with large r_s region where $|\mathrm{F}\rangle$ is the ground state, and investigate the SDE spectra of $|\mathrm{F}\rangle$ in the TDHF framework. Note here that the HF single-particle energy of Eq. (9) reads now

$$\varepsilon_{0\uparrow}=\hbar\omega_c\left(\frac{1}{2}-\frac{3}{2}\sqrt{\frac{\pi}{2}}r_s\right),\quad \varepsilon_{0\downarrow}=\frac{1}{2}\hbar\omega_c,$$
$$\varepsilon_{1\uparrow}=\hbar\omega_c\left(\frac{3}{2}-\frac{5}{4}\sqrt{\frac{\pi}{2}}r_s\right),\quad \varepsilon_{1\downarrow}=\frac{3}{2}\hbar\omega_c, \tag{28}$$

showing that $\varepsilon_{1\uparrow}<\varepsilon_{0\downarrow}$ for $0.638<r_s$, as in Fig. 10.

Because there is no hole states for down-spin electrons in $|\mathrm{F}\rangle$ as shown in Fig. 10, $B(\boldsymbol{q})$ and $\mathcal{Y}$ vanish identically in the TDHF Eq. (7) to give

$$A(\boldsymbol{q})\mathcal{X}^{(n)}=E^{(n)}\mathcal{X}^{(n)}. \tag{29}$$

The TDHF dispersion of the lowest SDE, which is denoted as $E^{(\mathrm{SDE})}$, is shown in Fig. 11 for $r_s=3$ and $r_s=1.5$. The figure shows (i) that the system is stable at $r_s=3$ against the spin fluctuation and (ii) that at $r_s=1.5$ the dispersion is negative for $q<1.7l^{-1}$, signaling the instability between $r_s=3$ and $r_s=1.5$. Note that $E^{(\mathrm{SDE})}$ vanishes identically at $q=0$ because σ_- commutes with the Hamiltonian. By investigating the dispersion in detail, we have found that the onset of the instability is at $r_s=2.15$ and at the wave number $q\simeq 0.2l^{-1}$. This means that $|\mathrm{F}\rangle$ is a local minimum of $E[\rho]$ of Eq. (23) for $r_s>2.15$ only.

Here we observe the spin instability of $|\mathrm{F}\rangle$ as r_s decreases across $r_s=2.15$. This makes a clear contrast with the situation for $|\mathrm{P}\rangle$, where the instability is observed as r_s increases

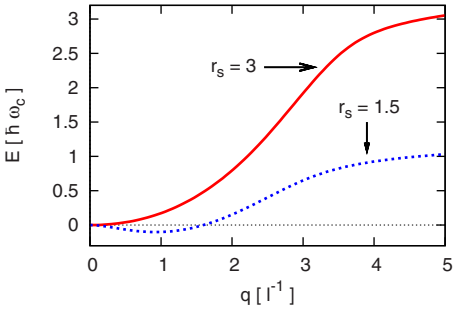

FIG. 11. (Color online) TDHF dispersion $E^{(\mathrm{SDE})}$ of the lowest SDE on $|\mathrm{F}\rangle$ in units of $\hbar\omega_c$ for $r_s=3$ and $r_s=1.5$.

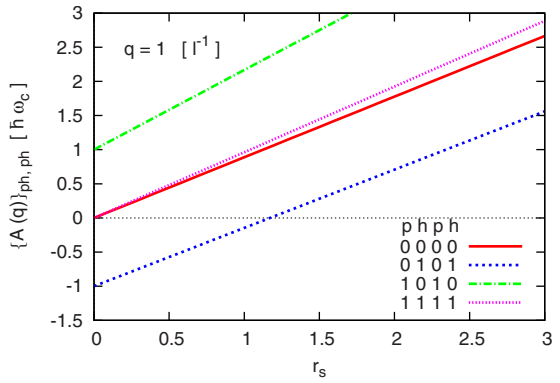

FIG. 12. (Color online) Diagonal component $\{A(\boldsymbol{q})\}_{ph,ph}$ in Eq. (29) in units of $\hbar\omega_c$ with $q=1.0l^{-1}$ as a function of r_s for $phph=(0000)$, (0101), (1010), and (1111). The lowest energy component, $\{A(\boldsymbol{q})\}_{01,01}$, becomes negative as r_s decreases, indicating possible spin instability.

across $r_s=2.01$. This difference can be explained using the r_s dependence of $A(\boldsymbol{q})$ in Eq. (29). In Fig. 12, we plot diagonal components $\{A(\boldsymbol{q})\}_{ph,ph}$ with $q=1.0l^{-1}$ as a function of r_s for several sets of indices. They are presented by straight lines because the Coulomb interaction is proportional to r_s, as shown in Eq. (2). Note here that particle states specified by p have $\sigma=\downarrow$, and hole states h have $\sigma=\uparrow$. Figure 12 shows clearly that $\{A(\boldsymbol{q})\}_{01,01}$ becomes negative as r_s decreases, approaching $-\hbar\omega_c$ at $r_s=0$. This implies that the ph excitation (particle$=0\downarrow$, hole$=1\uparrow$) becomes unstable (negative excitation energy) in the small r_s region, which in turn explains in an obvious way why we observe the spin instability as we decrease r_s.

Let us come to the q dependence of the dispersion in Fig. 11. We plot several examples of $\{A(\boldsymbol{q})\}_{ph,p'h'}$ for $r_s=1.5$ in Fig. 13. At $q=0$, only two ph components, $ph=(00),(11)$, are involved in the SDE, which are decoupled from other components at $q=0$ as is clear from Fig. 13. Then the relevant 2×2 matrix in Eq. (29) is given by $\{A(0)\}_{00,00}=\{A(0)\}_{11,11}=-\{A(0)\}_{00,11}=-\{A(0)\}_{11,00}$. This matrix gives vanishing excitation energy at $q=0$ as seen in Fig. 11. Here the eigenstate with vanishing energy is a coherent superposition of the two ph states, $ph=(00),(11)$. If we increase q,

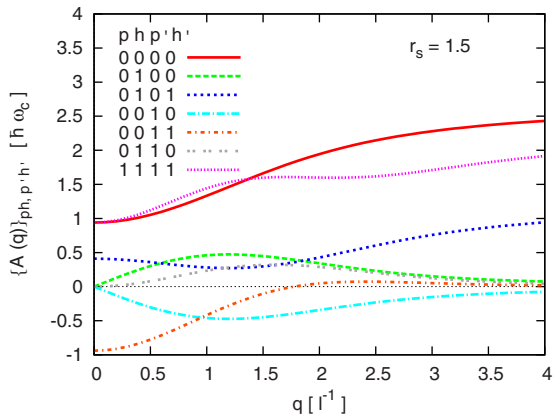

FIG. 13. (Color online) $\{A(\boldsymbol{q})\}_{ph,p'h'}$ in Eq. (29) in units of $\hbar\omega_c$ for several sets of ph indices as a function of q for $r_s=1.5$.

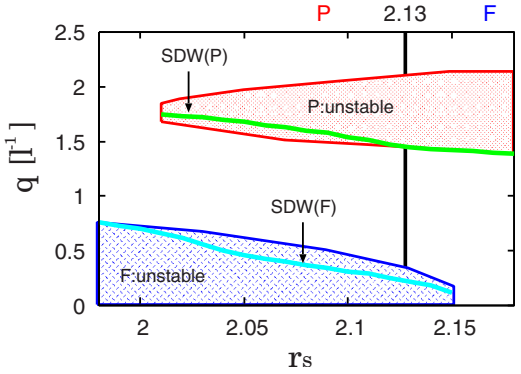

FIG. 14. (Color online) Area of spin instability for $E_Z=0$. The paramagnetic state $|\mathrm{P}\rangle$ is unstable in the shaded domain "P: unstable" with respect to the formation of SDW with wave number q. For each value of r_s, the lowest SDW energy is realized with the value of q on the line "SDW(P)." The instability of the ferromagnetic state $|\mathrm{F}\rangle$ is displayed in the same manner. On the vertical line at $r_s=2.13$, we have $E_\mathrm{P}=E_\mathrm{F}$.

other components come into play. At $r_s=1.5$, we see that $\{A(\boldsymbol{q})\}_{01,01}$, the lowest diagonal component of $\{A(\boldsymbol{q})\}$, is positive in the whole range of q, though it lowers with decreasing r_s as shown in Fig. 12. For finite q, however, $ph=(01)$ component couples with higher components, $ph=(00),(11),\ldots$, to change $\{A(\boldsymbol{q})\}_{01,01}$ into the negative dispersion in Fig. 11.

By combining the above findings with the results in Sec. III A, we have understood that neither $|\mathrm{P}\rangle$ nor $|\mathrm{F}\rangle$ is the ground state for $2.01<r_s<2.15$.

IV. GROUND STATE FOR $E_Z=0$

We perform the HF calculation in Sec. II C to obtain the new HF ground state to replace $|\mathrm{P}\rangle$ ($|\mathrm{F}\rangle$) where $|\mathrm{P}\rangle$ ($|\mathrm{F}\rangle$) is unstable. Then we compare all the obtained HF solutions to determine the ground state.

A. $|\mathrm{SDW(P)}\rangle$

Here we examine how the SDW replaces $|\mathrm{P}\rangle$ for $r_s>2.01$. We first exhibit the area of spin instability of $|\mathrm{P}\rangle$ in the (r_s,q) plane in Fig. 14. The area denoted by "P: unstable" shows that $|\mathrm{P}\rangle$ is unstable there, i.e., a point (r_s,q) in that area indicates that the paramagnetic state $|\mathrm{P}\rangle$ with the r_s value is unstable with respect to the SDE of the wave number q. Suppose we start from $|\mathrm{P}\rangle$ and increase r_s. Then Fig. 14 shows that we observe the onset of the spin instability at $r_s=2.01$ for $q\sim1.8l^{-1}$, which is in accordance with the TDHF results shown in Fig. 8.

For each value of $r_s(>2.01)$, we have looked for the ordering wave number q that minimizes the energy of the SDW solution. The optimal q is presented by the solid line denoted by "SDW(P)" in Fig. 14. In the following, we denote the SDW state on the line SDW(P) as $|\mathrm{SDW(P)}\rangle$, and its energy as $E_{\mathrm{SDW(P)}}$, indicating that it is an SDW that derives from $|\mathrm{P}\rangle$. We present $E_{\mathrm{SDW(P)}}$ in Fig. 15 together with E_P and E_F, to which we shall soon come back.

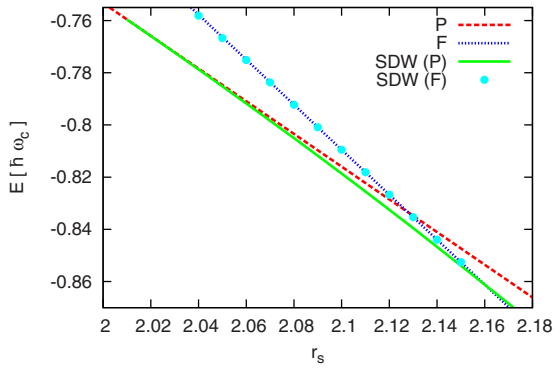

FIG. 15. (Color online) Energies of the four HF solutions, E_{P}, E_{F}, $E_{\mathrm{SDW(P)}}$, and $E_{\mathrm{SDW(F)}}$ for $E_Z=0$. Because $E_{\mathrm{SDW(F)}}(<E_{\mathrm{F}})$ is almost degenerate with E_{F} on this scale, it is presented by dots.

B. $|\mathrm{SDW(F)}\rangle$

Next we investigate the SDW that is to take the place of $|\mathrm{F}\rangle$ for $r_s<2.15$. It is easy to apply the HF framework in Sec. II C with minor modifications to the SDW that derives from $|\mathrm{F}\rangle$. The results are presented in Figs. 14 and 15, where we have defined $|\mathrm{SDW(F)}\rangle$ and $E_{\mathrm{SDW(F)}}$ in the same way as for the paramagnetic case.

We see in Fig. 14 that both $|\mathrm{SDW(F)}\rangle$ and $|\mathrm{SDW(P)}\rangle$ are the local minima of $E[\rho]$ in some range of r_s. It should be stressed, however, that $|\mathrm{SDW(F)}\rangle$ and $|\mathrm{SDW(P)}\rangle$ are different states. Roughly speaking, $|\mathrm{SDW(P)}\rangle$ at $r_s=2.13$, for example, is a condensate of $\sigma_+(\boldsymbol{q})$ and $\sigma_-(-\boldsymbol{q})$ bosons with $q\sim 1.5l^{-1}$ on $|\mathrm{P}\rangle$, while $|\mathrm{SDW(F)}\rangle$ is a condensate of $\sigma_-(\boldsymbol{q})$ boson with $q\sim 0.2l^{-1}$ on $|\mathrm{F}\rangle$.

C. Ground state for $E_Z=0$

Having obtained four solutions to the HF equation, we are now ready to compare their energies E_{P}, E_{F}, $E_{\mathrm{SDW(P)}}$, and $E_{\mathrm{SDW(F)}}$ in Fig. 15 to determine the lowest energy solution for each r_s. We then conclude that the system is in $|\mathrm{P}\rangle$ for $r_s<2.01$, $|\mathrm{SDW(P)}\rangle$ for $2.01<r_s<2.15$, and $|\mathrm{F}\rangle$ for $2.15<r_s$, which is shown in Fig. 16. Though E_{F}, $E_{\mathrm{SDW(P)}}$, and $E_{\mathrm{SDW(F)}}$ are almost degenerate at $r_s\sim 2.15$, we have confirmed that $|\mathrm{SDW(F)}\rangle$ cannot be the ground state for any value of r_s. Note that the transition at $r_s=2.01$ between $|\mathrm{P}\rangle$ and $|\mathrm{SDW(P)}\rangle$ is of second order because it follows a softening of the SDE on $|\mathrm{P}\rangle$. On the other hand, the transition at $r_s=2.15$ between $|\mathrm{F}\rangle$ and $|\mathrm{SDW(P)}\rangle$ is clearly of first order.

D. What is $|\mathrm{SDW(P)}\rangle$?

We have found that the system is in $|\mathrm{SDW(P)}\rangle$ for $2.01<r_s<2.15$, which we examine in some detail.

FIG. 16. (Color online) Phase diagram for $E_Z=0$. The transition $|\mathrm{P}\rangle\leftrightarrow|\mathrm{SDW(P)}\rangle$ at $r_s=2.01$ is of second order, and $|\mathrm{SDW(P)}\rangle\leftrightarrow|\mathrm{F}\rangle$ is of first order.

TABLE I. Single-particle states $(j=1,2)$ occupied in $|\mathrm{SDW(P)}\rangle$ at $r_s=2.13$, $q=1.45l^{-1}$. Some of the coefficients $D_{\alpha\uparrow,j}$ and $D_{\alpha\downarrow,j}$ are listed. The second column shows the eigenenergy ϵ_j of Eq. (19). Without the Coulomb interaction, $\epsilon_j=0.5\hbar\omega_c$ for $j=1,2$.

	ϵ_j $(\hbar\omega_c)$	$D_{0\uparrow,j}$	$D_{0\downarrow,j}$	$D_{1\uparrow,j}$	$D_{1\downarrow,j}$
$j=1$	−2.84	0.69	0.69	0.15	−0.15
$j=2$	−1.86	0.62	−0.62	−0.31	−0.31

Here we consider a typical example of $|\mathrm{SDW(P)}\rangle$ at $r_s=2.13$, which is defined at $q=1.45l^{-1}$ as shown by the line SDW(P) in Fig. 14. In this case, $|\mathrm{SDW(P)}\rangle$ is obtained by filling $j=1,2$ states of Eq. (20) which are defined by the coefficients $D_{\alpha\uparrow,j}$ and $D_{\alpha\downarrow,j}$ given in Table I. To be explicit, these two states $(j=1,2)$ can be written as

$$|j=1,k\rangle = 0.69|0\uparrow k+q_y\rangle + 0.69|0\downarrow k\rangle + \cdots,$$

$$|j=2,k\rangle = 0.62|0\uparrow k+q_y\rangle - 0.62|0\downarrow k\rangle + \cdots,$$

which shows that the mixture of up and down-spin states are very large.

With the coefficients in Table I, we can calculate the density matrix of Eq. (21) for the above $|\mathrm{SDW(P)}\rangle$, which we present in Table II. Then the expectation value of the spin operators given in Eq. (22) is easily obtained; we find that the $|\mathrm{SDW(P)}\rangle$ at $r_s=2.13$, $q=1.45l^{-1}$ is featured by

$$\langle\psi_\uparrow^\dagger(\boldsymbol{r})\psi_\uparrow(\boldsymbol{r})\rangle = \langle\psi_\downarrow^\dagger(\boldsymbol{r})\psi_\downarrow(\boldsymbol{r})\rangle = \frac{1}{2\pi l^2},$$

$$\langle\psi_\uparrow^\dagger(\boldsymbol{r})\psi_\downarrow(\boldsymbol{r})\rangle \sim 0.588\frac{1}{2\pi l^2}e^{-i\boldsymbol{q}\cdot\boldsymbol{r}}, \tag{30}$$

which are tabulated in Table III with $E_Z\neq 0$ cases. Note that the symmetric nature of the density matrix in Table II, which can be traced back to the degeneracy of the SDE in the $\sigma_\pm$ channels. This means that $|\mathrm{SDW(P)}\rangle$ is made by a condensate of σ_+ and σ_- bosons with equal weights. This is realized by the first line of Eq. (30) that gives $\langle\sigma_z\rangle=0$. This implies that the transition from $|\mathrm{P}\rangle$ to $|\mathrm{SDW(P)}\rangle$ does not tend to $|\mathrm{F}\rangle$. The second line of Eq. (30) shows that $|\mathrm{SDW(P)}\rangle$ at $r_s=2.13$ is a spiral SDW (Ref. 16) with the wave vector $q=1.45l^{-1}$.

TABLE II. Density matrix $\rho_{\alpha\sigma,\alpha'\sigma'}(q)$ of $|\mathrm{SDW(P)}\rangle$ at $r_s=2.13$, $q=1.45l^{-1}$ for several sets of (α,α') and (σ,σ').

ρ	↑↑	↑↓	↓↑	↓↓
00	0.85	−0.09	−0.09	0.85
01	−0.08	0.30	−0.30	0.08
10	−0.08	−0.30	0.30	0.08
11	0.12	−0.07	−0.07	0.12
02	−0.04	−0.12	−0.12	−0.04
20	−0.04	−0.12	−0.12	−0.08

TABLE III. Spin densities of the SDW at each E_Z in units of $1/2\pi l^2$. While $\langle\psi_\uparrow^\dagger\psi_\downarrow\rangle$ depends strongly on r_s and E_Z, $\langle\psi_\uparrow^\dagger\psi_\uparrow\rangle = \langle n_\uparrow\rangle$ is almost independent of E_Z (look at the data for $r_s=2.01$).

E_Z	r_s	q	$\langle\psi_\uparrow^\dagger\psi_\downarrow\rangle$	$\langle\psi_\uparrow^\dagger\psi_\uparrow\rangle$
0	2.01	1.75	0.110	1.00000
	2.13	1.45	0.588	1.00000
0.02	2.01	1.75	0.115	1.00032
	2.08	1.60	0.434	1.00652
0.04	2.01	1.75	0.128	1.00079
	2.04	1.69	0.294	1.00480

E. How can $|\mathrm{SDW(P)}\rangle$ gain energy ?

Here we examine how the system gains energy by making the second-order transition from $|\mathrm{P}\rangle$ to $|\mathrm{SDW(P)}\rangle$ on the basis of Eq. (23).

Let us look at $E_{\mathrm{SDW(P)}}$ and E_{P} in Fig. 17, which are decomposed into E_1, E_2, and E_3 as in Eq. (23). Here E_1 represents the kinetic energy, and E_2 and E_3 are the exchange energies. Note that E_3 derives from the mixture of $a^\dagger_{\alpha\uparrow}(k+q_y)$ and $a^\dagger_{\alpha\downarrow}(k)$ as given in Eq. (20), and is absent in E_{P}. Figure 17 shows that E_1 and E_2 of $E_{\mathrm{SDW(P)}}$ are higher than those of E_{P}. However, the gain in E_3 exceeds the loss in E_1 and E_2 to make $|\mathrm{SDW(P)}\rangle$ the ground state for $2.01<r_s<2.15$.

In order to understand the above mechanism, we study the system at $r_s=2.13$, which is $|\mathrm{SDW(P)}\rangle$ for $1.43l^{-1}<q<2.08l^{-1}$. In Fig. 18, we present $E[\rho]$ of Eq. (23) as a function of q. We see that the system can tune the density matrix ρ by becoming $|\mathrm{SDW(P)}\rangle$ to compensate the loss in E_1 and E_2 by the gain in E_3 in $1.43l^{-1}<q<2.08l^{-1}$. This is the same mechanism that we have seen as a function of r_s in Fig. 17. Let us look into E_3 in some detail. In Fig. 19, we present several terms that contribute to E_3 in Eq. (23). We realize

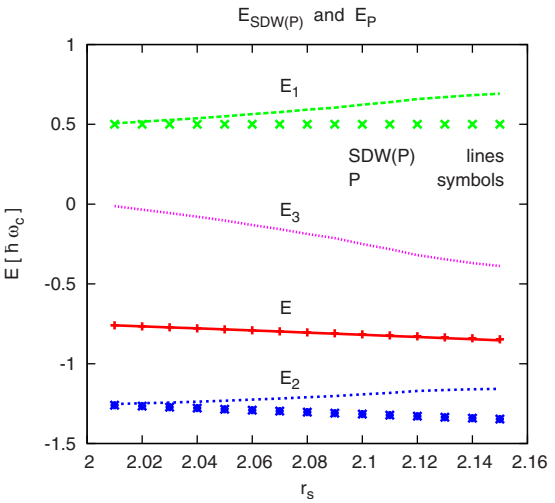

FIG. 17. (Color online) r_s dependence of $E_{\mathrm{SDW(P)}}$ (lines) and E_{P} (symbols). They are given by $E[\rho]$ of Eq. (23), and are decomposed into the kinetic energy E_1, and the exchange energy E_2 and E_3. Note that $E_{\mathrm{SDW(P)}}<E_{\mathrm{P}}$ for $2.01<r_s<2.15$, though they are degenerate on this scale.

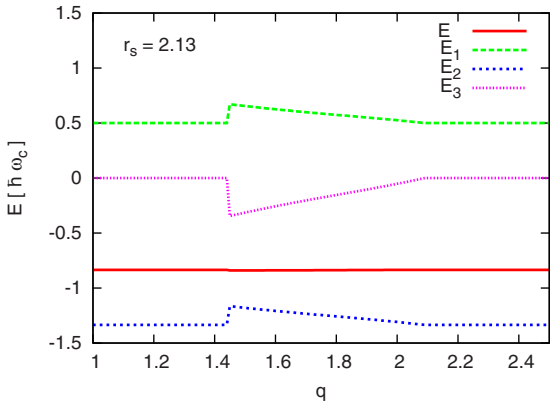

FIG. 18. (Color online) q dependence of $E[\rho]$ of Eq. (23) on the vertical line at $r_s=2.13$ in Fig. 14. It is decomposed as $E=E_1+E_2+E_3$ as in Fig. 17. The SDW phase is realized for $1.43l^{-1}<q<2.08l^{-1}$. Note that the minimum point of the total energy E, though hardly visible on this scale, is given at $q=1.45l^{-1}$, which defines $E_{\mathrm{SDW(P)}}$ at $r_s=2.13$.

that the dip of $-X_{1010}(\boldsymbol{q})$ around $q\sim 1.3l^{-1}$ and the peak of $-X_{1100}(\boldsymbol{q})$ around $q\sim 1.7l^{-1}$, which are shown in Fig. 9, are the main origin of the large gain in E_3. In other words, the system makes the new HF basis by mixing two states with wave number k and $k+q_y$ to form the SDW so that it can fully exploit the attractive nature of $-X_{1010}(\boldsymbol{q})$ and $-X_{1100}(\boldsymbol{q})$ in the above momentum region.

It is impossible to exaggerate the importance of $X_{1010}(\boldsymbol{q})$ and $X_{1100}(\boldsymbol{q})$ in the present analysis. In the study of the SDE dispersion, these two terms explain the softening phenomena as the *ph* interaction. In the description of the SDW, on the other hand, they give the attraction as the Fock exchange energy. It is essential to realize the dual role played by these two terms, i.e., the softening of the SDE and the stabilization of the SDW.

V. INSTABILITY FOR $E_Z\neq 0$

In this section, we examine the effect of a finite Zeeman energy E_Z on the results obtained in Sec III.

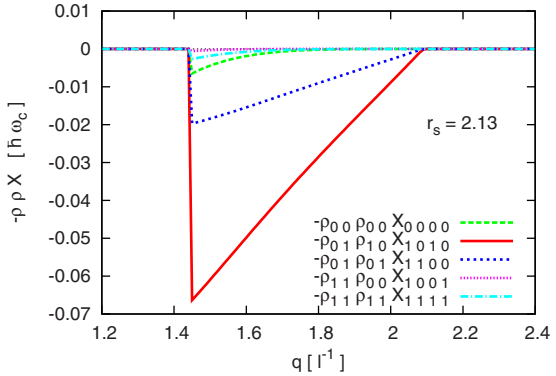

FIG. 19. (Color online) q dependence of main terms in E_3 of Eq. (23) at $r_s=2.13$. For example, the line denoted by $-\rho_{01}\rho_{01}X_{1010}$ stands for $-(1/2)\rho_{0\downarrow,1\uparrow}\rho_{1\uparrow,0\downarrow}X_{1010}(\boldsymbol{q})$ in Eq. (23). Note, for example, that $\rho_{10}\rho_{10}X_{1010}=\rho_{01}\rho_{01}X_{1010}$, which can be seen by the symmetry of ρ in Table II and that of $X_{\alpha\alpha'\beta\beta'}(\boldsymbol{q})$ in Eq. (A9).

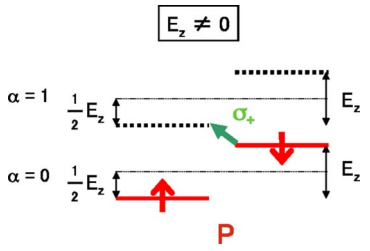

FIG. 20. (Color online) Schematical expression for the SDE on $|\mathrm{P}\rangle$ for $E_Z \neq 0$.

A. Instability of $|\mathrm{P}\rangle$ for $E_Z \neq 0$

We show pictorially the effect of the finite Zeeman energy $E_Z \neq 0$ on $|\mathrm{P}\rangle$ in Fig. 20. First, we realize that E_P is not dependent on E_Z because the effects of E_Z on the up-spin and down-spin electrons cancel out each other exactly. Second, we see that the SDE is not symmetric with respect to σ_+ and σ_- modes; the σ_+ mode is favored. In fact, all the unperturbed *ph* energies lower by E_Z in the σ_+ channel, and increase by E_Z in the σ_- channel. It is then easy to see that the TDHF equation for finite E_Z takes on the following form for the σ_+ mode:

$$\begin{pmatrix} A(\boldsymbol{q}) - E_Z & B(\boldsymbol{q}) \\ B^*(-\boldsymbol{q}) & A^*(-\boldsymbol{q}) + E_Z \end{pmatrix} \begin{pmatrix} \mathcal{X}^{(n)} \\ \mathcal{Y}^{(n)} \end{pmatrix} = (E^{(n)} - E_Z) \begin{pmatrix} \mathcal{X}^{(n)} \\ -\mathcal{Y}^{(n)} \end{pmatrix}. \tag{31}$$

It is obvious that the corresponding equation for the σ_- mode is obtained by changing $E_Z \to -E_Z$ in Eq. (31).

Comparing Eq. (7) for $E_Z=0$ and Eq. (31) for $E_Z \neq 0$, we realize a notable point: the eigenvector $(\mathcal{X}^{(n)}, \mathcal{Y}^{(n)})$ is common to Eqs. (7) and (31), while the eigenenergy is $E^{(n)}$ for Eq. (7) and $E^{(n)} - E_Z$ for Eq. (31). Let $E^{(\mathrm{SDE})}$ be the lowest eigenenergy given by Eq. (7). Then the onset of the spin instability of $|\mathrm{P}\rangle$ is given by $E^{(\mathrm{SDE})}=E_Z$ for $E_Z \neq 0$, and by $E^{(\mathrm{SDE})}=0$ for $E_Z=0$. Suppose we increase r_s from the high-density region where $|\mathrm{P}\rangle$ is the ground state. Then the above observation naturally leads us to the following points. First, $|\mathrm{P}\rangle$ becomes unstable at lower r_s for $E_Z \neq 0$ than for $E_Z=0$. Second, $E^{(\mathrm{SDE})}=E_Z(\neq 0)$ gives the instability of $|\mathrm{P}\rangle$ with respect to σ_+ mode only, i.e., σ_- mode is still stable at the critical point. This is in clear contrast to $E_Z=0$ case, where the instability for both σ_+ and σ_- modes occur simultaneously at $E^{(\mathrm{SDE})}=0$. The above asymmetry leads certainly to $\langle n_\uparrow \rangle \neq \langle n_\downarrow \rangle$ in the SDW state for $E_Z \neq 0$, as shall be shown later.

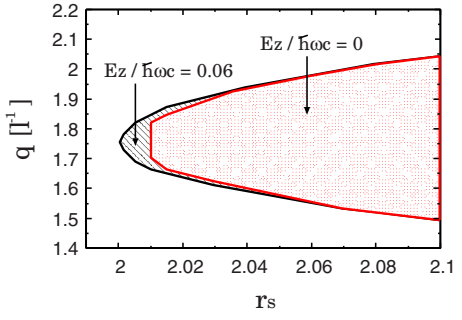

FIG. 21. (Color online) Domain of spin instability of $|\mathrm{P}\rangle$ for $E_Z/\hbar\omega_c=0$ (shaded area) and 0.06 (hatched area). The domain expands only very slowly with increasing E_Z.

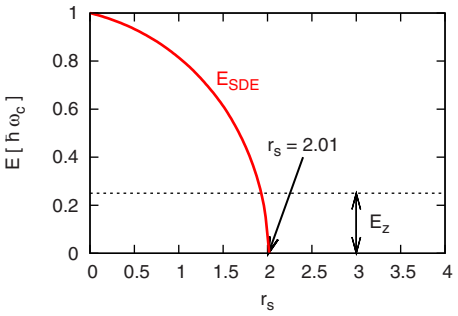

FIG. 22. (Color online) Minimum of the TDHF dispersion $E^{(\mathrm{SDE})}$ as a function of r_s. Transition point for $|\mathrm{P}\rangle \leftrightarrow |\mathrm{SDW(P)}\rangle$ is given by the intersection $E^{(\mathrm{SDE})}=E_Z$ shown in the figure. For $E_Z=0$, the transition point is $r_s=2.01$.

In Fig. 21, we show the area of spin instability of $|\mathrm{P}\rangle$ in the (r_s, q) plane for $E_Z=0$ and $0.06\hbar\omega_c$ in the same way as in Fig. 14. We realize that the domain of spin instability does expand as expected in the above, but only surprising slowly, with increasing E_Z. In other words, $|\mathrm{P}\rangle$ is quite stable against the Zeeman splittings. This can be explained by Fig. 22, which shows the minimum of the SDE dispersion on $|\mathrm{P}\rangle$ at $E_Z=0$ as a function of r_s, to display the softening of SDE shown in Fig. 8. We see that the excitation energy vanishes very rapidly in a nonlinear fashion as r_s approaches the critical value $r_s=2.01$ from below. Because the instability occurs at the intersection $E^{(\mathrm{SDE})}=E_Z$, Fig. 22 clearly shows that the critical value of r_s lowers very slowly as E_Z increases for $E_Z \lesssim 0.3\hbar\omega_c$. The above observation explains clearly the slow expansion of the domain of instability in Fig. 21. It also suggests that E_Z hardly affects the SDE boson that is to condensate, which shall be confirmed later in Sec. VI A.

B. Instability of $|\mathrm{F}\rangle$ for $E_Z \neq 0$

Here we consider the SDE on $|\mathrm{F}\rangle$ in the σ_- channel, which is depicted in Fig. 23. We can easily realize that the total energy per particle, E_F, of $|\mathrm{F}\rangle$ lowers by $E_Z/2$, and that all the unperturbed *ph* energies increase by E_Z. Then we realize that the TDHF equation for the SDE on $|\mathrm{F}\rangle$ is given by

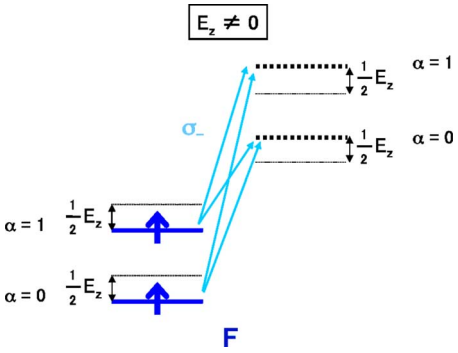

FIG. 23. (Color online) Schematical expression for the SDE on $|\mathrm{F}\rangle$ for $E_Z \neq 0$.

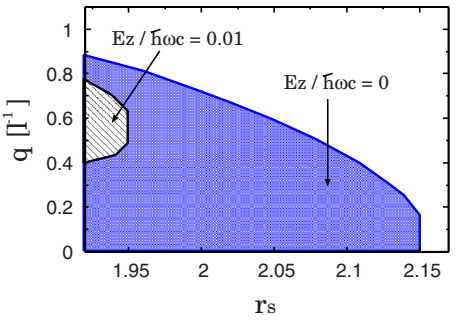

FIG. 24. (Color online) Domain of spin instability of $|\mathrm{F}\rangle$ for $E_Z/\hbar\omega_c=0$ (shaded area) and 0.01 (hatched area). The domain diminishes very rapidly with increasing E_Z, which should be compared with Fig. 21.

$$(A(\mathbf{q})+E_z)X^{(n)}=(E^{(n)}+E_z)X^{(n)}. \tag{32}$$

In the same way as for the paramagnetic case, Eqs. (32) and (29) have the same eigenvector $\mathcal{X}^{(n)}$ but with different eigenenergies $E^{(n)}+E_Z$ and $E^{(n)}$. In other words, the finite E_Z increases the excitation energy of SDE by E_Z without affecting its structure. This means that the finite E_Z suppresses the instability of $|\mathrm{F}\rangle$ and the realization of $|\mathrm{SDW(F)}\rangle$ as the ground state, compared to the $E_Z=0$ case in Fig. 10. This can be confirmed by Fig. 24, where the area of the instability of $|\mathrm{F}\rangle$ is shown in the (r_s,q) plane for $E_Z=0$ and $0.01\hbar\omega_c$, in the same way as in Fig. 21 for $|\mathrm{P}\rangle$. The domain of the spin instability shrinks very rapidly with increasing E_Z, which implies growing stability of $|\mathrm{F}\rangle$. Therefore, it is quite unlikely that $|\mathrm{SDW(F)}\rangle$ can be the ground state for a finite E_Z because it cannot be even at $E_Z=0$, as shown in Fig. 16. In fact, we shall see that there is no point on the (r_s,E_z) plane where $|\mathrm{SDW(F)}\rangle$ is the ground state.

VI. GROUND STATE FOR $E_Z\neq 0$

The HF calculation to obtain the SDW state for $E_Z\neq 0$ goes in the same fashion as for the $E_Z=0$ case in Sec. IV. Here we explain the HF solution for $|\mathrm{SDW(P)}\rangle$ and $|\mathrm{SDW(F)}\rangle$ for $E_Z\neq 0$.

A. $|\mathrm{SDW(P)}\rangle$ for $E_Z\neq 0$

We have performed the HF calculation in the whole domain of the spin instability in Fig. 21 for each value of E_Z, and have determined $|\mathrm{SDW(P)}\rangle$ and $E_{\mathrm{SDW(P)}}$ as a function of r_s and E_Z. We show $E_{\mathrm{SDW(P)}}$ in Fig. 25 together with

$$E_{\mathrm{P}}=\frac{1}{2}\hbar\omega_c\left(1-\sqrt{\frac{\pi}{2}}r_s\right),$$

$$E_{\mathrm{F}}=\hbar\omega_c\left(1-\frac{11}{16}\sqrt{\frac{\pi}{2}}r_s\right)-\frac{1}{2}E_Z, \tag{33}$$

for several values of E_Z. We realize that $E_{\mathrm{SDW(P)}}$ for a fixed value of r_s decreases very slowly with increasing E_Z. In fact, $E_{\mathrm{SDW(P)}}$ decreases by around one hundredth of E_Z, while E_{F} lowers exactly by $E_Z/2$.

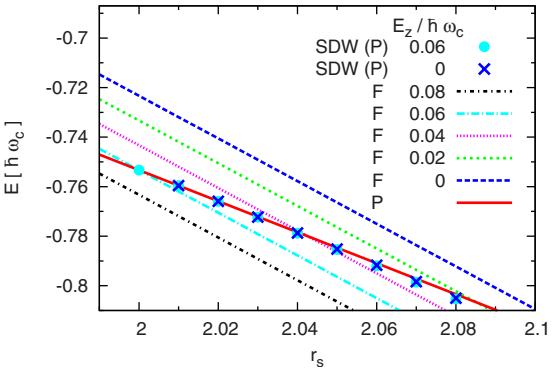

FIG. 25. (Color online) Total energy per electron E_{P}, E_{F}, and $E_{\mathrm{SDW(P)}}$ in each phase in units of $\hbar\omega_c$ for several values of E_Z. $E_{\mathrm{SDW(P)}}$ is only slightly dependent on E_Z, and is given for $E_Z/\hbar\omega_c=0$ and 0.06 only. The onset of $|\mathrm{SDW(P)}\rangle$ is $r_s=2.05$ for $E_Z/\hbar\omega_c=0$, and $r_s=2.00$ for $E_Z/\hbar\omega_c=0.06$, respectively. Though $E_{\mathrm{SDW(P)}}(E_Z=0.06\hbar\omega_c)<E_{\mathrm{SDW(P)}}(E_Z=0)$, they are degenerate on this scale.

The above point can be explained by examining the spin densities of $|\mathrm{SDW(P)}\rangle$ using Eq. (22). The results are listed in Table III together with the $E_Z=0$ case. It is remarkable that $\langle n_\uparrow\rangle=\langle\psi_\uparrow^\dagger\psi_\uparrow\rangle\simeq 1/(2\pi l^2)$ is hardly affected by E_Z, while $\langle\psi_\uparrow^\dagger\psi_\downarrow\rangle$ is strongly dependent on E_Z and r_s. In other words, E_Z does not reform the structure of the condensating boson, as was suggested by comparison of Eqs. (7) and (31) in Sec. V A; it just changes the amount of the condensate. The fact $\langle n_\uparrow\rangle\simeq\langle n_\downarrow\rangle$ also explains that $E_{\mathrm{SDW(P)}}$ is quite insensitive to E_Z; the effect of E_Z should cancel out each other between up and down-spin electrons.

The following point should be stressed at the end. One might have expected naively that $|\mathrm{SDW(P)}\rangle$ would change into $|\mathrm{F}\rangle$ with increasing E_Z. However, our result, $\langle n_\uparrow\rangle\simeq\langle n_\downarrow\rangle$ independently of E_Z, denies the above naive expectation.

B. $|\mathrm{SDW(F)}\rangle$ for $E_Z\neq 0$

We have performed the HF calculation to obtain $|\mathrm{SDW(F)}\rangle$ and $E_{\mathrm{SDW(F)}}$ in the whole domain of the spin instability in Fig. 24 for each value of E_Z. We plot $E_{\mathrm{SDW(F)}}$ in Fig. 26 together with E_{P} and E_{F} of Eq. (33). It is notable that the onset of $|\mathrm{SDW(F)}\rangle$ is $r_s=2.15$ for $E_Z=0$, and $r_s=1.95$ for $E_Z=0.01\hbar\omega_c$, showing that the onset of $|\mathrm{SDW(F)}\rangle$ moves quite quickly to the smaller r_s region with increasing E_Z, in accordance with Fig. 24. By combining the above observation with the fact that $E_{\mathrm{SDW(P)}}$ lowers slightly with increasing E_Z as shown in Fig. 25, we can conclude that $|\mathrm{SDW(F)}\rangle$ cannot be the ground state at any point on the (r_s,E_Z) plane.

VII. RESULTS AND DISCUSSIONS

Here we present the main result of this work, the phase diagram on the whole (r_s,E_Z) plane that is to replace Fig. 1. Then we compare our results with other theories and experimental results.

A. Phase diagram

Having understood that $E_{\mathrm{SDW(F)}}$ is not the lowest energy in any case, we now compare E_{P}, E_{F}, and $E_{\mathrm{SDW(P)}}$ to deter-

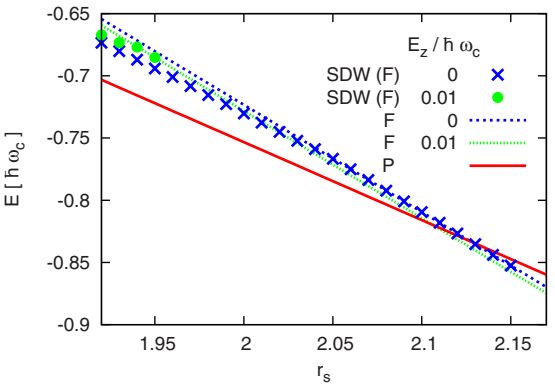

FIG. 26. (Color online) Total energy per electron E_P, E_F, and $E_{SDW(F)}$ in each phase in units of $\hbar\omega_c$ for several values of E_Z. The onset of $|SDW(F)\rangle$ is $r_s=2.15$ for $E_Z/\hbar\omega_c=0$, and $r_s=1.95$ for $E_Z/\hbar\omega_c=0.01$, respectively.

mine the ground state in the whole (r_s, E_Z) plane. The result is summarized on the phase diagram shown in Fig. 27.

In order to explain the main features of the diagram, we need only to know how the three energies, E_P, E_F, and $E_{SDW(P)}$, move with increasing E_Z, which is given in Fig. 25. We see (i) that E_P is not dependent on E_Z, (ii) that E_F decreases exactly by $E_Z/2$, and (iii) that $E_{SDW(P)}$ lowers only slightly. Then, we can explain Fig. 27 as follows.

First, let us consider how the boundary value of r_s between $|P\rangle$ and $|SDW(P)\rangle$ moves with increasing E_Z. Figure 25 shows that the onset of $|SDW(P)\rangle$ moves slightly to the smaller r_s direction ($r_s=2.01$ for $E_Z=0$, and $r_s=2.00$ for $E_Z=0.06\hbar\omega_c$). This explains the line in Fig. 27 that extends from ($r_s=2.01$, $E_Z=0$) upwards slightly to the left to ($r_s=2.00$, $E_Z=0.06\hbar\omega_c$).

Second, Fig. 25 shows that the intersection of E_F and $E_{SDW(P)}$ moves quickly to the smaller r_s direction with increasing E_Z. This explains the line in Fig. 27 that goes from ($r_s=2.15$, $E_Z=0$) to ($r_s=2.00$, $E_Z=0.06\hbar\omega_c$); $|SDW(P)\rangle$ is taken over by $|F\rangle$ promptly with increasing E_Z.

Third, for $E_Z/\hbar\omega_c \gtrsim 0.06$, $|SDW(P)\rangle$ cannot be the ground state for any value of r_s, as can be seen from Fig. 25. Then, $|P\rangle$ or $|F\rangle$ becomes the ground state according to $E_F \gtrless E_P$. The boundary is fixed by $E_P=E_F$, which is given by virtue of Eq. (33) as the straight line

$$\frac{E_Z}{\hbar\omega_c} = 1 - \frac{3}{8}\sqrt{\frac{\pi}{2}}r_s, \tag{34}$$

that goes from ($r_s=2.00$, $E_Z=0.06\hbar\omega_c$) to ($r_s=0$, $E_Z=\hbar\omega_c$).

Fourth, for $E_Z/\hbar\omega_c > 1$, $|F\rangle$ is the ground state for any value of r_s, i.e., $E_F < E_P$ for any r_s.

Let us summarize the above results. For $0 \le E_Z/\hbar\omega_c \le 0.06$, we have three phases $|P\rangle$, $|F\rangle$, and $|SDW(P)\rangle$ as in the case of $E_Z=0$. The boundary between $|P\rangle$ and $|SDW(P)\rangle$ is the second-order transition, and the boundary between $|F\rangle$ and $|SDW(P)\rangle$ is of first order. For $0.06 \le E_Z/\hbar\omega_c \le 1$, the first-order phase transition occurs between $|P\rangle$ and $|F\rangle$ at $E_P=E_F$. For $1 \le E_Z/\hbar\omega_c$, $|F\rangle$ is always the ground state.

At the end, it should be mentioned here that our investigation does not completely exclude other possibilities from the phase diagram. Here we have compared four probable phases, i.e., $|P\rangle$, $|F\rangle$, $|SDW(P)\rangle$, and $|SDW(F)\rangle$. If other phases are to be the ground state, however, they are not connected to either $|P\rangle$ or $|F\rangle$ by a second-order transition induced by the spin-density operator. Because the transition to such a phase does not accompany the softening of collective spin excitations, it would be difficult to find an evidence of such a phase by investigating excitation spectra experimentally.

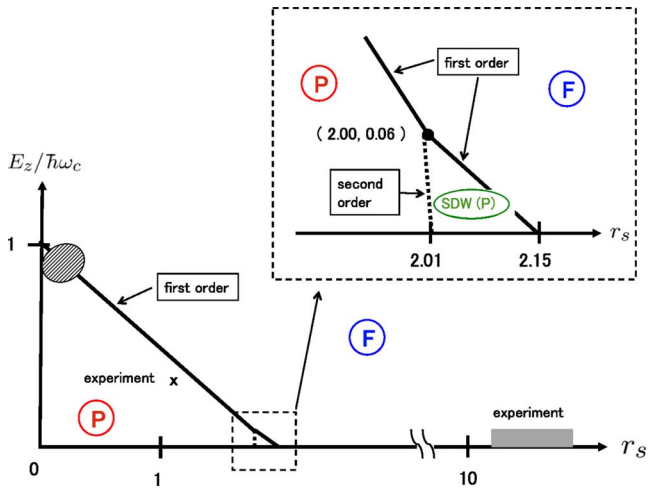

FIG. 27. (Color online) Magnetic phase diagram. Three phases, $|P\rangle$, $|F\rangle$, and $|SDW(P)\rangle$, are shown with their boundaries. In the hatched region, a first-order transition between $|P\rangle$ and $|F\rangle$ is expected theoretically (Refs. 6–8 and 10). The cross at ($r_s \sim 1.1, E_Z \sim 0.37\hbar\omega_c$) indicates the first-order transition observed experimentally (Refs. 25 and 26). Empirical SDE energy is expected to vanish in the shaded area ($11 \lesssim r_s \lesssim 14, E_Z \sim 0$) (Ref. 5).

B. Comparison with other theories

Here we compare our results with those of other approaches on the spin instability and the subsequent phase transition. Giuliani and Quinn studied the same system in the hatched area in Fig. 27, i.e., in the high-density ($r_s \ll 1$) and large Zeeman splitting ($E_Z \sim \hbar\omega_c$) regime, with a mean-field theory some time ago.[6–8] They concluded that the transition between $|P\rangle$ and $|F\rangle$ is of first order, and denied the possibility of the SDW ground state. This is in accordance with our results in the corresponding region in Fig. 27.

Another investigation of the present system was carried out by Park and Jain.[22] However, their results do not reproduce the transition between $|P\rangle$ and $|SDW(P)\rangle$ at $r_s=2.01$ for $E_Z=0$, which is confirmed both by the TDHF and HF calculations.[14,20] So we believe that their results cannot be compared directly with ours.

C. Comparison with experiment

In the high-density ($r_s \lesssim 1$) and large E_Z region, there are several empirical evidences that the $\nu=2$ paramagnetic system shows a first-order transition.[25–32] A clearly observed transition point ($r_s \sim 1.1, E_Z \sim 0.37\hbar\omega_c$) for $|P\rangle \leftrightarrow |F\rangle$ (Refs. 25 and 26) is marked by a cross in Fig. 27, which is quite

close to our phase boundary, indicating that the HF theory works well at $r_s \sim 1$.

In the low-density region, on the other hand, we do not have much empirical information. Some time ago, Eriksson *et al.*[5] performed inelastic-light-scattering experiment to explore the possible spin instability of $\nu=2$ system with $E_Z=0$, which is to take place at $r_s \sim 2$ (Refs. 14 and 20) in the HF theory as shown in Fig. 27. They observed (i) that the SDE dispersion shows softening with increasing r_s, but (ii) that the density at $r_s \sim 2$ is still too high to cause the spin instability. Though they could not find the instability, they suggested, by extrapolating their data to the low-density region, that the SDE energy tends to zero at $11 \lesssim r_s \lesssim 14$ to indicate a spin instability, which is shown as a shaded area in Fig. 27.

Qualitatively, main features of the above empirical findings are explained clearly by the present analysis of the SDE and the phase diagram; the softening of SDE spectra with increasing r_s is a precursor of the SDW, and the vanishing excitation energy of SDE marks the onset of SDW.

Quantitatively speaking, however, we notice several differences between our phase diagram and empirical findings. The experimental data suggest (i) that $|\mathrm{P}\rangle$ is the ground state in a wider area than obtained by the HF theory, i.e., the system is found to be $|\mathrm{P}\rangle$ up to $r_s \sim 6$ for $E_Z=0$,[5] and (ii) that the spin instability of which the onset is $r_s=2.01$ for $E_Z=0$ in the present HF theory is pushed into the lower density region $(11 \lesssim r_s \lesssim 14)$. A possible explanation is that fluctuations tend to prevent stabilization of $|\mathrm{F}\rangle$ and $|\mathrm{SDW(P)}\rangle$, which gain exchange energy by spin ordering. Another origin of the difference between our results and the available experimental data comes from the thickness of the real system, which is expected to shift the critical point of the spin instability to the lower-density region. For the system studied in the experiment,[5] it is expected that the finite thickness would push the critical point $r_s=2.01$ of the HF theory to $r_s \sim 3.3$.[5,33]

The above observation strongly suggests that the qualitative feature of our phase diagram in Fig. 27 is true in real systems. We believe that there are three phases, $|\mathrm{P}\rangle$, $|\mathrm{F}\rangle$, and $|\mathrm{SDW(P)}\rangle$, in the phase diagram. The following two limits are easily understood; (i) in the small r_s and small E_Z region, the system should be in $|\mathrm{P}\rangle$, and (ii) in the large r_s or large E_Z region, $|\mathrm{F}\rangle$ should be the ground state. On the phase boundaries, we have realized the following: first, there should be a first-order boundary between $|\mathrm{P}\rangle$ and $|\mathrm{F}\rangle$ that extends from $(r_s=0, E_Z/\hbar\omega_c=1)$ downwards to the right, which is confirmed both theoretically and experimentally, as shown Fig. 27. Second, it is quite likely that there is a second-order boundary between $|\mathrm{P}\rangle$ and $|\mathrm{SDW(P)}\rangle$ in the small E_Z region at $11 \lesssim r_s \lesssim 14$. We believe, from the above analysis and discussion, that the phase diagram of the real system should be obtained by shifting phase boundaries in the small E_Z region in Fig. 27 to the lower density side without affecting the qualitative structure of the phase diagram.

Experimental information is strongly awaited in three directions in connection with the SDW phase. The first one is the dispersion of the SDE on $|\mathrm{P}\rangle$ in the lower density region (down to $r_s \sim 10$) for $E_Z \sim 0$ to confirm the spin instability. The second one is to explore the SDW phase itself at $r_s \gtrsim 10$. The last one is the SDE on $|\mathrm{F}\rangle$ which would exhibit a softening for $E_Z \sim 0$, because $E_{\mathrm{F}} \sim E_{\mathrm{SDW(P)}} \sim E_{\mathrm{SDW(F)}}$ at $r_s \sim 2.15$ in the HF theory as shown in Fig. 15. It is also important to fix experimentally the line of the first-order transition $|\mathrm{P}\rangle \leftrightarrow |\mathrm{F}\rangle$ on the (r_s, E_Z) plane. We believe that experiments in these directions should elucidate interrelations between softening of the SDE dispersion, quantum phase transition to the SDW state, and its description as a condensate of the SDE boson.

VIII. CONCLUSION

To date, the phase diagram of the integer quantum Hall system on the (r_s, E_Z) plane has not been known in the mean-field theory even for the $\nu=2$ system, as shown in Fig. 1. In this situation, we have completed the phase diagram in Fig. 27 using the time-dependent Hartree-Fock (TDHF) and the Hartree-Fock (HF) theories in the following manner. First, we have looked for the onset of spin instabilities of the paramagnetic $|\mathrm{P}\rangle$ and ferromagnetic $|\mathrm{F}\rangle$ phases on the whole (r_s, E_Z) plane by examining the TDHF spectra of the spin-density excitation (SDE) in a systematic way, which in turn fixes possible second-order phase boundaries of $|\mathrm{P}\rangle$ and $|\mathrm{F}\rangle$. Second, we have performed the HF calculation to obtain a new HF ground state, the spin-density wave (SDW) indicated by the instability, where neither $|\mathrm{P}\rangle$ nor $|\mathrm{F}\rangle$ is stable. Our results are summarized in Fig. 27, which replaces Fig. 1. By comparing our results with available experimental data, we have argued that the phase diagram in Fig. 27 is consistent with empirical findings.

Important points we have made in the present analysis are the following. First, we have shown that the SDW is a stable ground state at $r_s \sim 2$ and $E_Z \sim 0$, which was denied by earlier works at $r_s \ll 1$ and $E_Z \sim \hbar\omega_c$. Second, we have shown that the structure of the SDW hardly changes with increasing E_Z. The naive expectation is thus denied that the SDW would tend to the ferromagnetic phase with increasing E_Z. Third, we have clarified that the Coulomb exchange interaction in a specific particle-hole channel plays a dual and important role in the whole scenario of the quantum phase transition: one is the softening of the SDE and the other is the stabilization of the SDW. We believe that the present work has made a clear step toward the full understanding of the integer quantum Hall system in a tilted magnetic field.

APPENDIX: MATRIX ELEMENTS

In this appendix, we briefly review the matrix elements of the Coulomb interaction $v(\boldsymbol{r}_1, \boldsymbol{r}_2)=e^2/|\boldsymbol{r}_1-\boldsymbol{r}_2|$ using the single-particle wave function $\psi_{\alpha k}(\boldsymbol{r})$ of Eq. (3) in the Landau gauge.

Let us first define the matrix element of $e^{i\boldsymbol{q}\cdot\boldsymbol{r}}$ with $\boldsymbol{q}=(q_x, q_y)=(q\cos\theta, q\sin\theta)$ as

$$\int d\boldsymbol{r}\, \psi^*_{\alpha k_1}(\boldsymbol{r}) e^{i\boldsymbol{q}\cdot\boldsymbol{r}} \psi_{\beta k_2}(\boldsymbol{r}) = \delta_{k_1-k_2, q_y} e^{-\frac{i}{2}(k_1+k_2)q_x l^2} F_{\alpha\beta}(\boldsymbol{q}). \tag{A1}$$

Here, $F_{\alpha\beta}(\boldsymbol{q})$ is a vertex function given by

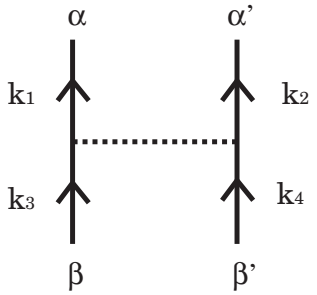

FIG. 28. Diagrammatic expression for $V_{\alpha\alpha'\beta\beta'}(k_1,k_2,k_3,k_4)$ of Eq. (A5).

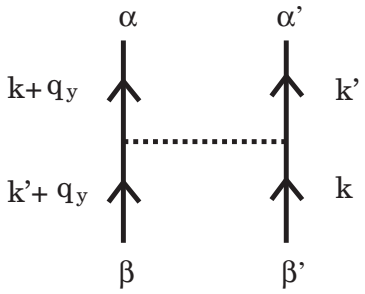

FIG. 29. Diagrammatic expression for the process that enters the definition of $X_{\alpha\alpha'\beta\beta'}(\boldsymbol{q})$ in Eq. (A7).

$$F_{\alpha\beta}(\boldsymbol{q}) = \mathcal{N}_\alpha \mathcal{N}_\beta^* e^{-i(\alpha-\beta)\theta} f_{\alpha\beta}(q), \tag{A2}$$

where $\mathcal{N}_\alpha = i^\alpha e^{-i\alpha\theta}$ is a phase factor that depends on the direction of $\boldsymbol{q}$, and $f_{\alpha\beta}(q)$ is defined using the Laguerre polynomial L (Ref. 34) as

$$f_{\alpha\beta}(q) = \sqrt{\frac{\beta!}{\alpha!}} e^{-q^2l^2/4} \left(\frac{ql}{\sqrt{2}}\right)^{\alpha-\beta} L_\alpha^{\alpha-\beta}\left(\frac{q^2l^2}{2}\right). \tag{A3}$$

Note that $f_{\beta\alpha}(q) = (-1)^{\alpha-\beta} f_{\alpha\beta}(q)$, and therefore that the following symmetry properties hold for the vertex function:

$$F_{\alpha\beta}(-\boldsymbol{q}) = (-1)^{\alpha-\beta} F_{\alpha\beta}(\boldsymbol{q}),$$

$$F_{\alpha\beta}^*(\boldsymbol{q}) = F_{\beta\alpha}(-\boldsymbol{q}). \tag{A4}$$

Now the matrix element of the Coulomb interaction in Fig. 28 can be written as[18–20]

$$V_{\alpha\alpha'\beta\beta'}(k_1,k_2,k_3,k_4) = \int d\boldsymbol{r}_1 d\boldsymbol{r}_2 \psi_{\alpha k_1}^*(\boldsymbol{r}_1)\psi_{\alpha' k_2}^*(\boldsymbol{r}_2) v(\boldsymbol{r}_1,\boldsymbol{r}_2) \times \psi_{\beta k_3}(\boldsymbol{r}_1)\psi_{\beta' k_4}(\boldsymbol{r}_2)$$

$$= \frac{1}{L}\delta_{k_1+k_2,k_3+k_4} V_{\alpha\alpha'\beta\beta'}(k_1-k_4,k_1-k_3), \tag{A5}$$

where $V_{\alpha\alpha'\beta\beta'}(k_1-k_4,k_1-k_3)$ is given in terms of the vertex function of Eq. (A2) as

$$V_{\alpha\alpha'\beta\beta'}(k,k') = \int \frac{d\boldsymbol{q}}{(2\pi)^2} 2\pi\delta(k'-q_y) \times e^{-ikq_xl^2} v(\boldsymbol{q}) F_{\alpha\beta}(\boldsymbol{q}) F_{\alpha'\beta'}^*(\boldsymbol{q}). \tag{A6}$$

Here $v(\boldsymbol{q}) = 2\pi e^2/q$ is the Fourier transform of the Coulomb interaction e^2/r in the 2D system.

In the study of the SDE in the TDHF framework, the following combination of matrix elements depicted in Fig. 29 appears naturally as the *ph* interaction:

$$e^{i\phi(k)} \sum_{k'} V_{\alpha\alpha'\beta\beta'}(k+q_y,k',k'+q_y,k) e^{-i\phi(k')} = X_{\alpha\alpha'\beta\beta'}(\boldsymbol{q}), \tag{A7}$$

where $\phi(k) = (k+q_y/2)q_xl^2$. By substituting Eqs. (A5) and (A6) in Eq. (A7), we obtain the following explicit form of $X_{\alpha\alpha'\beta\beta'}(\boldsymbol{q})$:

$$X_{\alpha\alpha'\beta\beta'}(\boldsymbol{q}) = \int \frac{d\boldsymbol{p}}{(2\pi)^2} e^{-i(\boldsymbol{p}\times\boldsymbol{q})_z l^2} v(\boldsymbol{p}) F_{\alpha\beta}(\boldsymbol{p}) F_{\alpha'\beta'}^*(\boldsymbol{p}). \tag{A8}$$

Then the symmetry property of $X_{\alpha\alpha'\beta\beta'}(\boldsymbol{q})$ can be easily derived from Eqs. (A4) and (A8) as

$$X_{\alpha'\alpha\beta'\beta}(\boldsymbol{q}) = X_{\alpha\alpha'\beta\beta'}(-\boldsymbol{q}) = (-1)^{\alpha+\alpha'+\beta+\beta'} X_{\alpha\alpha'\beta\beta'}(\boldsymbol{q}),$$

$$X_{\alpha\alpha'\beta\beta'}^*(\boldsymbol{q}) = X_{\beta\beta'\alpha\alpha'}(\boldsymbol{q}). \tag{A9}$$

In actual calculations, we have evaluated $X_{\alpha'\alpha\beta'\beta}(\boldsymbol{q})$ as follows. After performing the angular integral in Eq. (A8), we arrive at

$$X_{\alpha\alpha'\beta\beta'}(\boldsymbol{q}) = \frac{e^2}{l} \frac{\mathcal{N}_\alpha \mathcal{N}_{\alpha'}}{\mathcal{N}_\beta \mathcal{N}_{\beta'}} \int d\hat{p} \hat{f}_{\alpha\beta}(\hat{p}) \hat{f}_{\beta'\alpha'}(\hat{p}) J_{\alpha+\alpha'-\beta-\beta'}(\hat{p}\hat{q}), \tag{A10}$$

where J is the Bessel function. Here we have introduced dimensionless momentum variables $\hat{p} = pl$ and $\hat{q} = ql$, and the obvious notation $\hat{f}_{\alpha\beta}(\hat{p}) = f_{\alpha\beta}(p)$. Then the integral can be performed analytically using integral formulas with Bessel functions[34] as

$$\int d\hat{p}\hat{f}_{\alpha\beta}(\hat{p})\hat{f}_{\mu\nu}(\hat{p})J_{\lambda}(\hat{p}\hat{q}) = \sqrt{\frac{\beta!\,\nu!}{\alpha!\,\mu!}}\sqrt{\frac{\pi}{2}}\frac{1}{2^m}\frac{1}{(\sqrt{2})^{\lambda}}\frac{1}{\lambda!}\sum_{l=0}^{\beta}\frac{\alpha!\,(-1)^l}{(\alpha-\beta+l)!\,(\beta-l)!\,l!}\frac{1}{2^l}$$
$$\times\sum_{k=0}^{\nu}\frac{\mu!\,(-1)^k}{(\mu-\nu+k)!\,(\nu-k)!\,k!}\frac{1}{2^k}(2m+2l+2k-1)!!\,\hat{q}^{\lambda}F\left(m+l+k+\frac{1}{2},\lambda+1;-\frac{\hat{q}^2}{2}\right), \quad \text{(A11)}$$

where $\alpha\geq\beta$, $\mu\geq\nu$, $\lambda\geq 0$, and $\alpha-\beta+\mu-\nu+\lambda=2m$ and F is the confluent hypergeometric function defined by[34]

$$F(\alpha,\gamma;z) = 1+\frac{\alpha}{\gamma}\frac{z}{1!}+\frac{\alpha(\alpha+1)}{\gamma(\gamma+1)}\frac{z^2}{2!}+\cdots. \quad \text{(A12)}$$

As an immediate application of the above formula, we obtain, for example,

$$X_{0000}(0) = \frac{e^2}{l}\sqrt{\frac{\pi}{2}},$$
$$X_{1001}(0) = X_{1010}(0) = \frac{e^2}{l}\frac{1}{2}\sqrt{\frac{\pi}{2}},$$
$$X_{1111}(0) = \frac{e^2}{l}\frac{3}{4}\sqrt{\frac{\pi}{2}}. \quad \text{(A13)}$$

[1] *Perspectives in Quantum Hall Effects: Novel Quantum Liquids in Low-Dimensional Semiconductor Structures*, edited by S. D. Sarma and A. Pinczuk (Wiley, New York, 1997).
[2] D. Olego, A. Pinczuk, A. C. Gossard, and W. Wiegmann, Phys. Rev. B **25**, 7867 (1982).
[3] W. Hansen, M. Horst, J. P. Kotthaus, U. Merkt, C. Sikorski, and K. Ploog, Phys. Rev. Lett. **58**, 2586 (1987).
[4] A. Pinczuk, J. P. Valladares, D. Heiman, A. C. Gossard, J. H. English, C. W. Tu, L. Pfeiffer, and K. West, Phys. Rev. Lett. **61**, 2701 (1988).
[5] M. A. Eriksson, A. Pinczuk, B. S. Dennis, S. H. Simon, L. N. Pfeiffer, and K. W. West, Phys. Rev. Lett. **82**, 2163 (1999).
[6] G. F. Giuliani and J. J. Quinn, Phys. Rev. B **31**, 6228 (1985).
[7] G. F. Giuliani and J. J. Quinn, Solid State Commun. **54**, 1013 (1985).
[8] G. F. Giuliani and J. J. Quinn, Surf. Sci. **170**, 316 (1986).
[9] G. Murthy, Phys. Rev. Lett. **85**, 1954 (2000).
[10] A. Wójs and J. J. Quinn, Phys. Rev. B **65**, 201301(R) (2002).
[11] S. Yarlagadda, Phys. Rev. B **44**, 13101 (1991).
[12] K. Yoshizawa, N. Hirano, and K. Takayanagi, Phys. Rev. Lett. **91**, 066802 (2003).
[13] K. Yoshizawa and K. Takayanagi, Phys. Rev. B **71**, 125118 (2005).
[14] K. Yoshizawa and K. Takayanagi, Phys. Rev. B **76**, 155329 (2007).
[15] A. W. Overhauser, Phys. Rev. **128**, 1437 (1962).
[16] G. F. Giuliani and G. Vignale, *Quantum Theory of the Electron Liquid* (Cambridge University Press, Cambridge, 2005).
[17] A. H. MacDonald, Phys. Rev. B **30**, 4392 (1984).
[18] C. Kallin and B. I. Halperin, Phys. Rev. B **30**, 5655 (1984).
[19] C. Kallin and B. I. Halperin, Phys. Rev. B **31**, 3635 (1985).
[20] A. H. MacDonald, J. Phys. C **18**, 1003 (1985).
[21] I. K. Marmorkos and S. Das Sarma, Phys. Rev. B **45**, 13396 (1992).
[22] K. Park and J. K. Jain, J. Phys.: Condens. Matter **12**, 3787 (2000).
[23] D. W. Wang, S. Das Sarma, E. Demler, and B. I. Halperin, Phys. Rev. B **66**, 195334 (2002).
[24] P. Ring and P. Schuck, *The Nuclear Many-Body Problem* (Springer-Verlag, Berlin, 1980).
[25] S. Koch, R. J. Haug, K. v. Klitzing, and M. Razeghi, Phys. Rev. B **47**, 4048 (1993).
[26] S. Koch, R. Haug, K. von Klitzing, and M. Razeghi, Physica B **184**, 76 (1993).
[27] A. J. Daneshvar, C. J. B. Ford, M. Y. Simmons, A. V. Khaetskii, A. R. Hamilton, M. Pepper, and D. A. Ritchie, Phys. Rev. Lett. **79**, 4449 (1997).
[28] V. Piazza, V. Pellegrini, F. Beltram, W. Wegscheider, T. Jungwirth, and A. H. MacDonald, Nature (London) **402**, 638 (1999).
[29] V. Piazza, V. Pellegrini, F. Beltram, W. Wegscheider, M. Bichler, T. Jungwirth, and A. H. MacDonald, Physica E **6**, 108 (2000).
[30] L. V. Kulik, I. V. Kukushkin, V. E. Kirpichev, J. H. Smet, K. v. Klitzing, and W. Wegscheider, Phys. Rev. B **63**, 201402(R) (2001).
[31] L. V. Kulik, I. V. Kukushkin, S. Dickmann, V. E. Kirpichev, A. B. Van'kov, A. L. Parakhonsky, J. H. Smet, K. von Klitzing, and W. Wegscheider, Phys. Rev. B **72**, 073304 (2005).
[32] V. Piazza, V. Pellegrini, F. Beltram, and W. Wegscheider, Solid State Commun. **127**, 163 (2003).
[33] C. Kallin, in *Interfaces, Quantum Wells, and Superlattices*, edited by C. R. Leavens and R. Taylor (Plenum, New York, 1988), p. 163.
[34] I. S. Gradshteyn and I. M. Ryzhik, *Table of Integrals, Series, and Products*, 6th ed. (Academic, London, 2000).